HYDRODYNAMIC FOCUSED PASSIVE SEPARATION UNDER CONTINUOUS FLOW IN A MICROFLUIDIC CHIP

A thesis

presented to

the Faculty of California Polytechnic State University,

San Luis Obispo

In Partial Fulfillment

of the Requirements for the Degree of

Master of Science in Biomedical Engineering

by

Jad N. Kanbar

Committee Membership

TITLE: HYDRODYNAMIC FOCUCED PASSIVE
                                SEPARATION UNDER CONTINUOUS FLOW IN A
                                MICROFLUIDIC CHIP

AUTHOR: Jad N. Kanbar

DATE SUBMITTED: SEPTEMBER 2012

COMMITTEE CHAIR: David S. Clague, Ph.D.

                                Associate Professor, Biomedical and General Engineering

                                California Polytechnic State University, San Luis Obispo

COMMITTEE MEMBER: Lanny V. Griffin, Ph.D.

                                Professor and Chair, Biomedical and General Engineering

                                California Polytechnic State University, San Luis Obispo

COMMITTEE MEMBER: Richard N. Savage, Ph.D.

                                Professor and Chair, Materials Engineering

                                California Polytechnic State University, San Luis Obispo

Abstract

HYDRODYNAMIC FOCUCED PASSIVE SEPARATION UNDER CONTINUOUS FLOW IN A MICROFLUIDIC CHIP

Jad Kanbar

A continuous flow, passive separation device was designed using an equivalent circuit to create variable flow rates for hydrodynamic focusing to drain channels and collection outlets. By varying the diameter of the sample inlet connection into the reservoir, the particle position was influenced significantly, which enabled desired separations. Additionally it was noted that the relative, horizontal position of the inlet also had a significant influence on particle position within the device. A dimensionless number, the Characteristic Sample Inlet, was developed to relate geometric properties of the inlet reservoir to downstream particle distribution. It was found that a 2:1 ratio between inlet reservoir and sample inlet diameter, and placed at the top of the reservoir yielded the best separation results. Fluid velocity profiles in the reservoir were explored using Comsol Multyphysics. The experimentally observed particle trajectories and COMSOL predictions were in good agreement. Based on Comsol models a dimensionless parameter to relate the unique velocity profiles within the inlet reservoir to downstream separation of particles was also developed. A mixture of 10, 5.5, and 3.0 µm particles were separated to three distinct collection outlets at 73.4%, 64.7%, and 52.8% respectively. Therefore this project shows that passive separations of particles can be achieved simply by alerting the ratio of inlet hole relative to inlet reservoir diameter, and by placing the inlet hole at the top of the reservoir.

Keywords: Microfluidics, Passive Separation, Continuous Flow, COMSOL

Acknowledgements

I would like to give my sincere thanks and gratitude to Dr. Clague for his outstanding support throughout my time at Cal Poly. When I was first admitted to the Master's Program, he welcomed me with open arms to the Biomedical Engineering Department and in his group. I will never forget how much that meant to me, especially since I wanted nothing more than to work on microfluidics. He was there every time I needed an extra push, and always had great words of encouragement, with an eye towards developing my skill-set. I truly believe that my time with him has made me a much better researcher, scientist, and engineer.

I would like to thank Dr. Savage as well for his support. In his classroom and cleanroom I developed skills and analytical problem solving that have become fundamental building blocks for my beginning career. I know that every year a new set of students will go through the same steps I did, and much like me, they are incredibly lucky for the opportunities you give them.

I would also like to thank Dr. Griffin for being on my committee. I was given a wonderful opportunity to join the Biomedical Engineering Department and for that am extremely grateful. The students, faculty, and overall department atmosphere helped me grow tremendously both academically and professionally.

Lastly I would like to save my last thanks for my parents, Hiam and Nabih Kanbar. Words cannot describe how incredible they have been for me every step along the way. They have never hesitated to support any of my ideas, and always made sure that I followed through with any new goal until the end.

Table of Contents

List of Figures

List of Tables

I Introduction

1.1 Overview of Microfluidic Technology

Microfluidics in bioengineering can be considered a combination of fluid mechanics, surface chemistry, and biology [1]. By understanding and leveraging microscale phenomena, microfluidics can be used to perform separation techniques and experiments not possible on the macroscale, allowing new functionality and experimental paradigms to emerge [2]. The effects that become dominant in microfluidics include laminar flow, diffusion, surface area to volume ratio, and surface tension, to name a few [2]. These dominant characteristics make the designing of such devices unique and challenging. This project aimed to utilize the unique properties of microfluidics to design a device that has an ability to separate particulates of different diameters only using the suspending fluid flow without external fields.

At its core microfluidic devices have utilized many of the same fabrication steps already established in the semiconductor industry to produce microfluidic "chips" or Lab-on-a-Chip. The components of which can be rapid prototyped using the elastomer, poly(dimethylsiloxane) (PDMS) poured over a photoresist master mold on a silicon wafer [3]. This manufacturing strategy creates an exact replicate of intricate device features at the micron length scales. The benefit of using devices with channel widths that range from 1 to 1000 μm, while processing fluid volume that range from 10^{-9} to 10^{-18} liters are smaller reagent volumes, shorter reaction times, and the possibility of parallel operation [2, 3, 4].

The promise of integrating an entire laboratory onto a single chip involves the ability to design and fabricate devices to include components such as valves, pumps, mixers and switches [5]. To date, many types of micro-devices have been developed and thoroughly explored some of which include for example a cell culturing chip [6], protein crystallization chip [7], and electrophoretic DNA concentration and separation chip [8]. Microfluidics provides many potential applications in biological studies. The hope is that this technology may be introduced into the clinical health care domain. One such expectation is its role in pre-emptive healthcare or early detection of disease biomarkers while diseases are at the treatable stage [4]. Furthermore, a main driving force behind the development of Lab-on-Chip devices is that they open up the possible combination of practicality and ease of use by non-scientific experts such as first responders.

Microfluidic devices have been developing rapidly since the concept of fluid-integrated circuit, lab-on-a-chip, or micro-total-analysis system (μTAS) was introduced [9]. μTAS have expanded into a diverse number of analytical chemistry applications and has received a great amount of input from a wide spectrum of scientific and engineering disciplines [10]. For example, companies like Fluidigm and Caliper have begun to commercialize devices for large scale genotyping assays and enzyme activity analysis.In the so called μTAS, an entire analytical procedure can be performed, including sample pre-treatment, labeling reactions, separation, downstream reactions and detection on a portable chip [11]; however this idealized concept has seldom been realized due to the difficulties associated with the separation of target analytes from complex mixtures.

1.2 Batch and Continuous Separation Processes Applied To Microfluidics

Separation and filtration of microparticles based on size is essential for many applications such as biochemical and environmental assays, micro/nano-manufacturing, and clinical analysis [12]. The purification or separation of microparticles such as polymer beads, cells, emulsions, colloids, and airborne dust has become one of the main priorities of recent chemical, biomedical, and environmental studies as it represents an important step in many chemical and biological processes [9, 13]. Separation processes most commonly used in microfluidic applications can be broadly categorized in two main categories based on the method of sample volume introduction, i.e. batch and continuous flow processes.

Shown in Figure 1A, batch processes are separations carried out after the precise injection of a small sample volume. In batch procedures a particular volume of sample that is injected undergoes a separation process, and the separation time is plotted versus signal [11]. Batch processes include filtration, centrifugation and most prominently, forms of chromatography and electrophoresis. An issue with these types of processes type is that the efficiency of separation can only be evaluated after the process has finished, preventing mid-process adjustments such as altering flow speeds, carrier liquid composition, or instrumental parameters [11]. This approach therefore can make the separation process more labor intensive; i.e., experiments must be conducted to identify optimal conditions. Additionally, this complicates upstream or downstream applications preventing potential "in-line" integration with other device components a μTAS would require [11].

As shown in Figure 1B, continuous flow separations are carried out while the sample is introduced into a system that has a continuous buffer and/or sample. Theoretically, multiple samples can be processed on chip using continuous flow processes because the separation occurs without interruption. In such systems, a force is typically applied at an angle relative to the fluid flow to deflect target solutes within the flow to different paths toward specific device channels. A single outlet channel or many outlet channels can be fabricated to accommodate collection of any number of separated particles. A number of forces have been used in continuous separation processes including electric or magnetic fields, as well as standing ultrasonic waves and/or the intelligent design of flow obstacles [11].

In contrast to batch processes the separation efficiency in a continuous process can be tracked in real-time with immediate feedback. Hence adjustment of the experimental conditions can be performed while the process is still in progress and the detection signal is plotted versus position [11]. Therefore continuous separation not only facilitates incorporation into an integrated microfluidic system but also enables high-throughput processes [10]. This results in faster detection analysis and reuse. Lastly separation of particles in a continuous process requires no labeling because the process exploits a particle's inherit characteristic such size or charge.
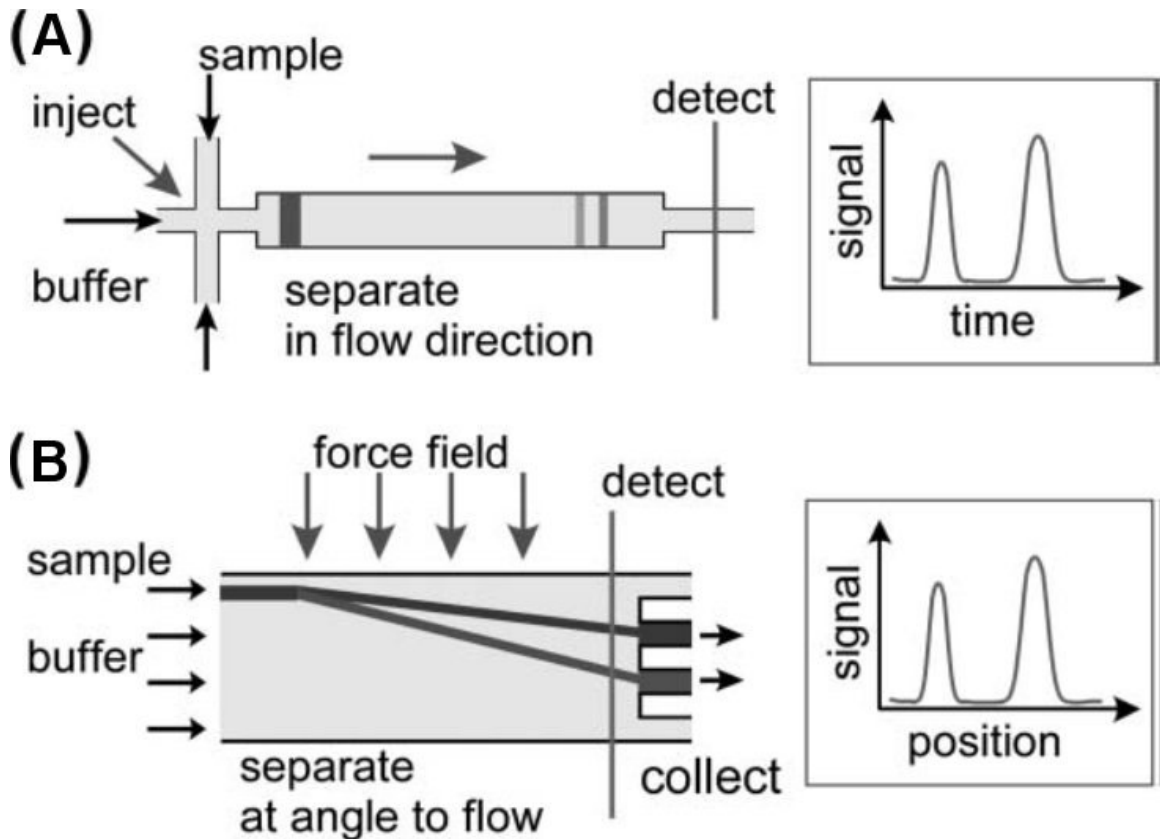
Figure 1. Diagrams demonstrating the differences between a batch separation and continuous separation [12].

In the above figure, (a) batch separation detection signal is plotted relative to time, whereas (b) in a continuous process, detection signal is plotted relative to position.

1.3 Project Goal and Benefit of Using a Passiveover Active Separation Processes

The main goal of the project was to develop a continuous flow microfluidic separation device for a mixture of microparticles of different diameters. This device however would achieve separation without the aid of an external field, but passively using only unique channel design and control of hydrodynamic flow. In general continuous flow separation techniques in the microscale can be subdivided into two broad categories, active and passive separation methods. The difference between the two approaches lies in the nature of the field source applied to produce the separation. In

active separations a force is applied by an external field, usually at a perpendicular angle to the flow stream. Examples of these forces include a homogenous electric field used in electrophoresis, a pH gradient for isoelectric focusing, an inhomgenous magnetic field for magnetophoresis, and an acoustic standing wave for acoustophoresis [11]. Up to 100,000 cells/hr can be sorted using electrokinetic flow control [14], switch valves [15], electrostatic force [16], dielectrophoresis [17], or optical manipulation [13, 18]. These systems, however, require fluorescence-labeled particles as well as optical sensing devices, making them too complex for ease of use, especially outside a laboratory setting [13]. Although the separation accuracy is high in these methods, particle separation requires a relatively long preparation time and since the process may not be continuous, it is not suitable for higher throughput preparation of particles [19]. Consequently the more complex the separation technique, the greater training any operator is required to obtain.

The dependence on particle charge and mobility presents constraints on the type of solutes that can be analyzed with some of these active separation techniques [20]. Additionally, incorporating external forces in a device not only increases its complexity, but also may limit an ability to function on biological samples damaging biological macromolecules and cells, causing cell lysis. External fields can have significant power requirements, as in the case for dielectrophoresis typically where alternating (AC) electric fields of 10 kHz to 100 MHz are applied [17]. These additional components can be much larger than the chip, such as high frequency power amplifier, hence negating some of the advantages of chip base microfluidic processes. Lastly the device fabrication may be complex and difficult to integrate with other downstream or upstream components required in a μTAS.

Passive separation methods can get around technical and design problems associated with active separation. They have received significant attention in the past decade due to the discoveries of many interesting fluid dynamic phenomena in microfluidics [9]. With an appropriate microfluidic design and control of hydrodynamic flow, it is possible to force microparticles or cells into specific flow stream lines and to separate these objects [11]. A simple system is certainly preferable if it must be incorporated into a microfluidic system as a unit operation only requiring low voltage syringe pumps [13]. In this project only two syringe pumps were needed and after their attachment to the microfluidic chip, no additional setup was required. This is a significant improvement in equipment requirement over electrophoretic or dielectrophoretic separations. Although this method does not allow for 100% separation efficiency, it is a very effective way of enriching particle concentrations according to size [11]. As comparison, up to 12,000 particles/hr can be processed and separated using the passive separation device developed in this project. Additionally the ability to separate particles without chemical or physical manipulation using fluorescence labels or large external forces makes the device ideal for biological samples such as small eukaryotic or bacterial cells with a range in diameter from 10 to 3.0 µm. Most important though, for integration in a µTAS, a continuous flow passive separation device can easily be placed downstream of sample purification and concentration, and upstream of sample detection and analysis.

1.4 Theoretical Principle of Passive Microfluidic Separation Devices

At the microscale physical phenomena of fluid and particles in suspension behave much differently than in the macroscale. This in turn directly governs the mechanism and theory behind a microfluidic passive separations device. Dimensionless numbers are routinely used in microfluidics to describe this fluid and particle phenomena. The Reynolds number (Re) describes the ratio of inertial to viscous forces acting on the fluid, and is used to delineate fluid flow regimes, e.g., laminar versus turbulent flow:

$$Re = \frac{\rho v D_H}{\mu} \tag{1}$$

where ρ is the fluid density, v is the characteristic fluid velocity, μ is fluid viscosity and D_H is the hydraulic diameter based on the cross-sectional channel geometry. Typically a Reynolds number above 2300 characterizes turbulent fluid flow with chaotic and unpredictable stream line flow patterns. At a Reynolds of ~2300, fluid streamlines become more ordered, and a transition to laminar flow occurs, with a Re < 2300. Laminar flow is a condition in which the trajectory of an undisturbed particle in a fluid stream follows the stream lines of the flow [2]. Mixing does not occur when two streams characterized by laminar flow are side by side; the only mixing that does occur is by diffusion at the interface between streams. For example, when two streams in the laminar flow regime introduced into a common channel, the fluids form an interface and species transport occurs by diffusion across that interface; hence mixing in microflows is an active area of research.

The Reynolds number compares the magnitude of inertial and viscous force densities [21]. Viscous forces depend on the fluid viscosity, which resists motion, and inertial forces depend on fluid momentum. When viscous forces dominate, solvent and solute particles do not cross stream-lines during flow. When inertial forces dominate, solvent and solute particles do cross stream lines. Since volume forces such as inertia and gravity are proportional to volume, these forces become negligible at the micron scale [22]. However, surface forces such as viscosity and surface tension do become dominant at the micron scale [22]. This implies that viscous forces dominate at the low Reynolds number regimes of laminar flow. Inertia rarely plays a significant role in microfluidic systems, and as systems are made ever smaller, it becomes even less relevant [21].

A particle suspended in a flowing fluid is affected by both inertial and viscous forces via interaction with the fluid [9]. The particle Reynolds number (Re_p) can be used to estimate the relative importance of these two forces, viz:

$$Re_p = \frac{U_m a^2 \rho_f}{D_H \mu}. \tag{2}$$

where U_m is the maximum flow velocity in the channel, a is particle diameter, and ρ_f is the density of the fluid. In a microchannel when the $Re_p \ll 1$, the particulate flow is dominated by viscous interactions and thus particles at rest are accelerated to the local fluid velocity owing to viscous drag of the fluid over the particle surface [23]. Since in passive, continuous flow separation devices, no externally applied field is added, the drag force tends to be the most important force controlling the particle motion [12]:

$$F_D = 6\pi \mu a U_P. \tag{3}$$

9

where U_p is the particle velocity. At low Reynolds number the flows are slow enough that particle diffusion becomes important. The dimensionless number that describes the importance of convection to diffusion is the Peclet number (Pe). The Pe number is defined as the ratio of advection rate to diffusion rate and is used in mass transport to estimate particle motion:

$$Pe = \frac{UD_H}{D} \tag{4}$$

where D is the diffusion coefficient of the particle, and U is the average velocity of the fluid. In situations where the Pe >> 1, convection or advection of the fluid flow dominates over diffusive affects [9].

1.5 Operational Principle of the Passive Microfluidic Device

By utilizing the theoretical principles of particulates in a microfluidic device derived above, a passive separations chip was designed and implemented. The goal of the chip was to passively separate three micron sized particulates into three distinct channels. To improve on experimental throughput, a symmetrical design was employed. Figure 2 is a schematic diagram showing an overview of the microfluidic chip with position labels demonstrating particulate migration and fluid flow in the entire device.

At position [1] of Figure 2, particles where introduced into the device through a sample inlet placed at different locations relative to the inlet reservoir. At position [2], particles were then able to migrate along different trajectories out of the reservoir based on their preferred streamline due to the total drag force as result of Stokes Flow (see

Figure 2). Buffer streams at position [3] hydrodynamically focused the microspheres exiting the Inlet Reservoir (see Figure 2). Position [4] highlights the part of the chip that will now be described as the "bifurcation segment" (also see Figure 3). At this position, the outer streams of the sheath flow due to hydrodynamic focusing carried out roughly 80% of the flow rate to the drain outlet channels. The focused stream carried out the remaining flow rate, roughly 20% to the bifurcation segment. The bifurcation segment split into three Collection Outlets on both sides. Lastly at position [5], particles of different diameters were collected to three Collection Outlets labeled **1**, **2** and **3** in Figure 2.

Particles that were initially positioned near to or along the wall of the inlet reservoir at position [2], eventually distributed to Collection Outlet 1 (see Figure 2). These particles tended to have the largest diameter. Particles positioned at the center of the inlet reservoir resulted in Collection Outlet 3. These particles tended to have the smallest diameter. Finally particles with an intermediate diameter and trajectory resulted in Collection Outlet 2.
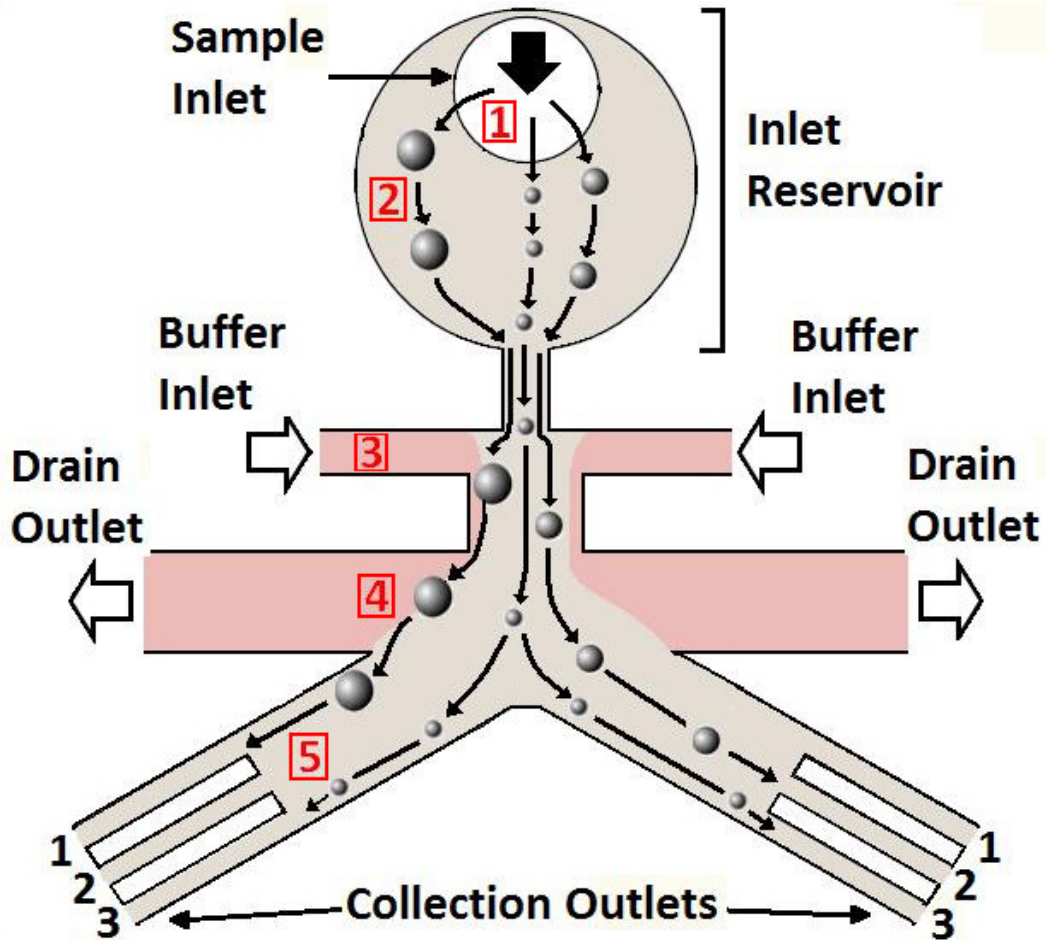
Figure 2. A schematic diagram demonstrating the principles of the passive separation device (not drawn to scale). There are two inlets: Sample and Buffer. There are eight outlets: two Drain, and three Collections on both sides. At position [1], particulates are introduced, and at position [2] these particulates migrate along different trajectories in the Inlet Reservoir. Buffer Inlet streams at position [3] focused the particles to the bifurcation segment at position [4]. The outer sheath flow at position [4] exits to the Drain Outlets, and the middle focused flow containing the particulates flowed to the Collection Outlets. At position [5], particles of three different diameters were collected to three separate Collection Outlets 1, 2, and 3.

1.6 Theoretical Principle at the Bifurcation Segment of the Microfluidic Device

Figure 3 is an enlarged schematic view of the bifurcation segment; this drawing is not drawn to actual scale. As described above, particles at position [3] were focused to the bifurcation segment by intersecting buffer streams (see Figure 2 and 3). At position

12

[4], the sudden abrupt presence of the drain channels on both sides of the device pushed particles laterally towards the drain channels. However this lateral distance was too small for particles to exit towards the drain channels. Instead particles moved through the bifurcation, separating to Collection Outlets **1**, **2**, and **3** at position [5] (see Figure 3).

The lateral distance to which particles migrated at position [4], was due to a momentum streamline change resulting from a lateral inertial force. This force points outwards in the direction of the drain channels and is indicated in Figure 3 as $\mathbf{F_L}$. The Inertial Lateral Force, $\mathbf{F_L}$, is given by:

$$F_{Lateral} \sim \frac{\rho_d \pi d^3 U^3}{6 D_h} \tag{6}$$

where ρ_p is the particle density, d is the particle diameter, U is average fluid velocity, D_h is the characteristic hydraulic diameter. The inertial force is balanced by the Stokes Drag Force, and thus equation (6) can be rearranged to solve for the lateral migration velocity of the particle, U_d:

$$U_{Lateral} \sim \frac{\rho_d d^2 U^2}{18 \mu D_h}. \tag{7}$$

Bifurcation Segment
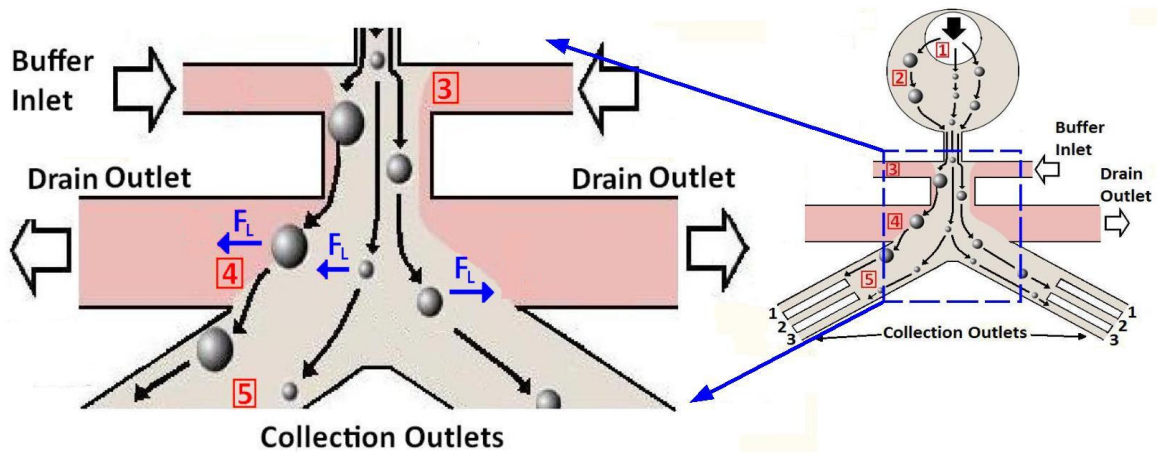
Figure 3. An expanded schematic diagram of the bifurcation segment demonstrating particle movement and direction of the lateral inertial force (drawing not drawn to scale). On the right, a segmented blue box over the device indicates the bifurcation segment. Buffer Inlet streams at position [3] focused the particles to position [4]. The outer sheath flow at position [4] exits to the Drain Outlets, and the middle focused flow containing the particulates flowed to the Collection Outlets. The presence of the drain channels created a streamline momentum change pushing particles outward laterally indicated by the blue arrows, due to an induced inertial force, F_L. The particles continued to flow through the bifurcation to position [5], where particles of three different diameters were collected to three separate Collection Outlets 1, 2, and 3.

II Methods

2.1 Device Design

2.1.1 Design Using an Equivalent Circuit Model

To design all microfluidic devices in this projected an equivalent circuit model was utilized. With this model an entire device and flow rate ratios through each channel could be defined. To arrive at these defined geometries a derivation is presented below. In the microscale, pressure drop from laminar flow in channel with rectangular cross-section is given by the Hagen–Poiseuille equation [24]:

$$\Delta P = \frac{32U\mu L}{D^2} \tag{8}$$

where ΔP is the pressure drop, U is the average fluid velocity, μ is the fluid viscosity, L is the length of the channel and D is the hydraulic diameter of specific microchannel geometry. Pressure drop is proportional to average fluid velocity and the length of the channel. In a rectangular channel, the hydraulic diameter D is given by:

$$D = \frac{2wd}{w + d} \tag{9}$$

where w is the width of the channel, and d is the depth of the channel. Flow rate Q, is given by this next equation:

$$Q = Uwd. \tag{10}$$

15

If equation (8) is rearranged and solved for average velocity, U, these variables can be substituted into equation (10) to get:

$$Q = \Delta P \times \frac{D^2 wd}{32\mu L} \tag{11}$$

The second term in equation (11) is defined as the inverse of hydraulic resistance R in a microchannel. Substituting this concept of hydraulic resistance into equation (4) transforms to:

$$Q = \Delta P \times \frac{1}{R} \tag{12}$$

For all the microfluidic designs in this project, the pressure drop from inlet to each outlet is the same in all channels. In other words, the pressure drop from the inlets to drain channel or from the inlets to any collection outlet is equal. With this, flow rate in equation (12) can be proportionally reduced to the inverse hydraulic diameter:

$$Q \propto \frac{1}{R} \propto \frac{D^2 wd}{L} \tag{13}$$

Flow rate is then dominated by hydraulic diameter D, width of the channel w, depth of the channel d, and length of the channel L. For these following calculations, the constant terms from equation (11) are dropped. The total flow rate Q_T into the device is the same as the total flow rate out. To take advantage of this in the design of the devices, Q_T was defined as the same sum of the drain channel outlet flow rate Q_D, and collection outlet flow rate Q_o:

16

$$Q_T = Q_D + Q_O \tag{14}$$

The proportion of total flow rate to the outlet channels was defined for two cases - the proportion of total flow rate Q_T, to the drain channel Q_D and the proportion of total flow rate Q_T, to the collection outlet channels Q_o. These proportions are given below:

$$0.8\, Q_T = Q_D \tag{15}$$

$$0.2\, Q_T = Q_O \tag{16}$$

where 80% of Q_T was designed to flow out of the drain channels and 20% of Q_T was designed to flow out of the collection outlets. If equations (15) and (16) are combined together, they form:

$$0.25\, Q_D = Q_O \tag{17}$$

where the collection outlet flow rate was 25% of the drain channel flow rate. The collection outlet channel had two segments with differing width geometries. As shown in Figure 4, there is a beginning part of the collection channel that did not split, followed by the portion of the channel that split into three distinct collection outlet channels 1, 2, and 3. Thus the flow rate to the collection outlets is given by:

$$Q_O = Q_{O1} + Q_{O2} \tag{18}$$

where Q_{O1} is the flow rate at beginning of the collection channel, and Q_{O2} is the combined split flow rate out the collection outlets (i.e. Outlet 1, 2, and 3 on both sides of the device). Since total flow rate is proportional to the inverse of hydraulic resistance, equation (18) can be written as:

$$Q_T \propto \frac{1}{R_D} + \frac{1}{R_O} \tag{19}$$

Furthermore, hydraulic resistance through the drain channel is then given by:

$$R_D = \frac{L_D}{D_D^2 w_D} \tag{20}$$

where L_D is the length of the drain channel, w_D is width of the drain channel, and D_D is the hydraulic diameter of the drain channel as shown in Figure 4. The parameter of depth is dropped out of the hydraulic resistance equation because it is equal in all channels. The hydraulic resistance through the collection outlet is given by:

$$R_O = R_{O1} + R_{O2} \tag{21}$$

where R_{O1} is the hydraulic resistance through the initial segment of the collection outlet and R_{O2} is the hydraulic resistance through all the split channels of the collection outlet as shown in Figure 4. The hydraulic resistances of R_{O1} and R_{O2} are thus given by:

$$R_{O1} = \frac{L_{O1}}{D_{O1}^2 w_{O1}} \tag{22}$$

$$R_{O2} = 3 \left(\frac{L_{O2}}{D_{O2}^2 w_{O2}} \right) \tag{23}$$

where L_{O1} and L_{O2} are channel lengths in the collection outlet, w_{O1} and w_{O2} are the widths of the channels through in the collection outlet, and D_{O1} and D_{O2} are the hydraulic diameters in the collection outlet respectively. Combining equations (22) and (23) into equation (21), the hydraulic equation through the collection outlet gives:

$$R_O = \frac{L_{O1}}{D_{O1}^2 w} + \frac{3D_{O2}^2 w_{O2}}{L_{O2}} \tag{24}$$

Now that expressions were derived for the hydraulic resistance through all the channels, equations (20) and (24) substituted into the total flow rate equation (12) to give:

$$Q_T \propto \frac{D_D^2 w}{L_D} + \frac{D_{O1}^2 w}{L_{O1}} + \frac{3D_{O2}^2 w_{O2}}{L_{O2}} \tag{25}$$

where all the geometric parameters of the device are included into oneequation. This equation was then used to design all parts of the microfluidic device. In the design of all the devices L_{O2}, the length of the collection outlets was chosen as an unknown variable. All other geometric parameters in equation (25) were given initial values. To solve for L_{O2}, Equations (15) and (20) were substituted into equation (25) and rearranged to give:

$$L_{O2} = 3D_{O2}^2 w_{O2} \left(\frac{1}{0.25 \, \frac{D_D^2 w_D}{L_D}} - \frac{L_{O1}}{D_{O1}^2 w_{O1}} \right) \tag{26}$$

Tables 1 displays channel lengths including L_{O2} for each device, Table 2 displays channel widths for each device, and Table 3 displays the hydraulic diameters for each device. With every geometric parameter then accounted for; the devices were designed in AutoCAD.
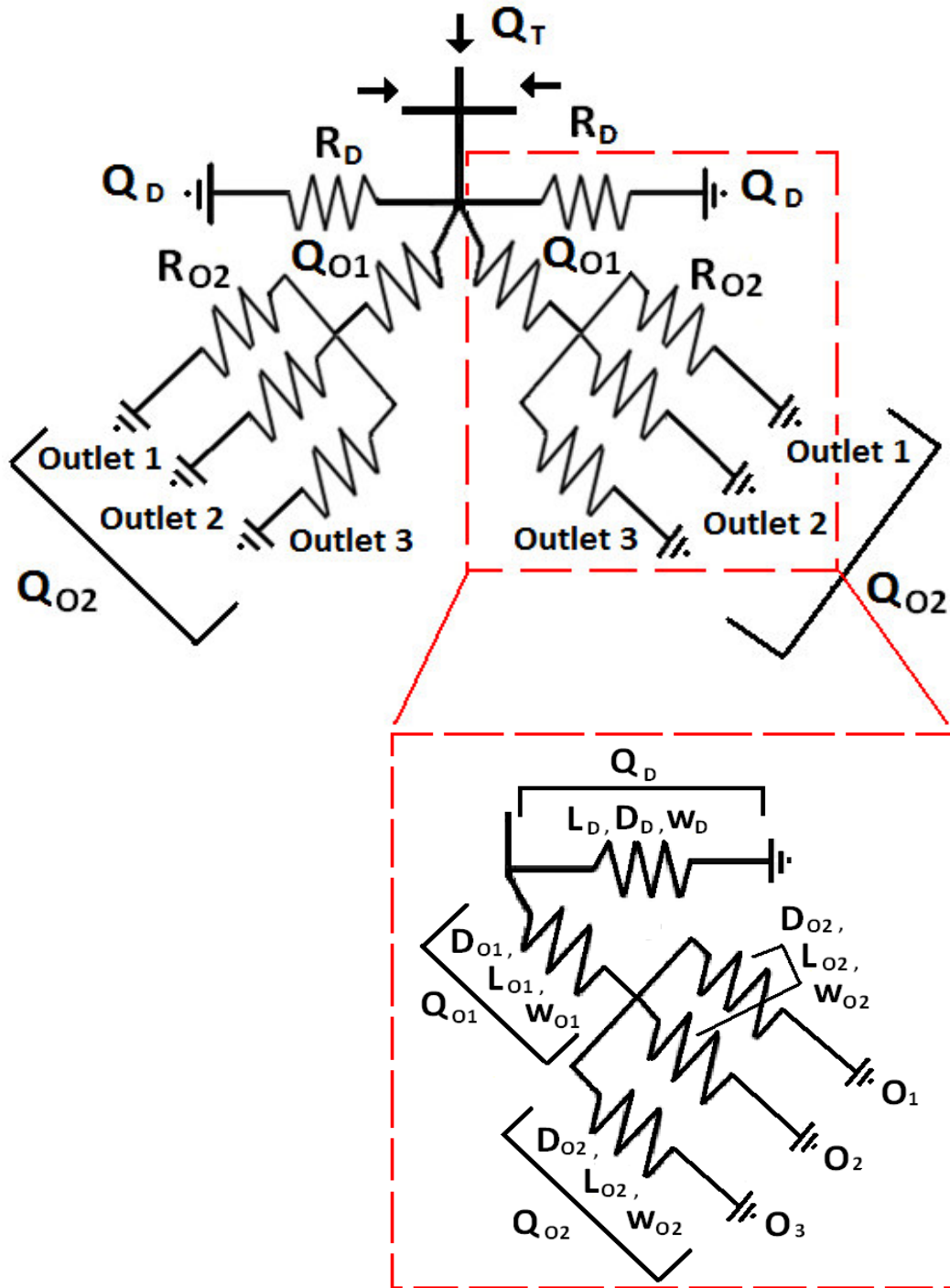
Figure 4. A schematic of an Equivalent Circuit Design used for all representative microfluidic devices.

All microfluidic chips were designed using the above parameters (See Text for definitions of variables). An Expanded View of one side showing a Drain and Collection Channels are shown to help identify the specific locations of Channel Lengths, Widths, and Hydraulic diameters. The Collection Outlets (O1, O2, and O3) originate from one Channel width (Q_{O1}) and split into three channels (Q_{O2}).

Table 1. Exact Length of All Outlet Channels Used in each Chip Design

Chip Design	Drain Channel Length, L_D (µm)	Collection Outlet Length, L_{O1} (µm)	Collection Outlet Length, L_{O2} (µm)	Channel Depth, d (µm)
1	2500	1250	3287	25
2	2000	2000	3254	25
3	2000	2000	3753	25

Table 2. Exact Widths of All Outlet Channels Used in each Chip Design

Chip Design	Drain Channel Widths, w_D (µm)	Outlet Channel Width, w_{O1} (µm)	Outlet Channel Width, w_{O2} (µm)
1	200	200	46.7
2	350	350	90.0
3	500	500	133.3

Table 3. Exact Hydraulic Diameters of All Outlet Channels Used in each Chip Design

Chip Design	Drain Hydraulic Diameter, D_D (µm)	Outlet Hydraulic Diameter, D_{O1} (µm)	Outlet Hydraulic Diameter, D_{O2} (µm)
1	44.4	44.4	32.6
2	46.7	46.7	39.1
3	47.6	47.6	42.1

2.1.2 Drawing the Transparency Mask in AutoCAD

AutoCAD^{TM} 2007 was used to draw all the devices based on the geometric parameters determined using the Equivalent Circuit Design model.
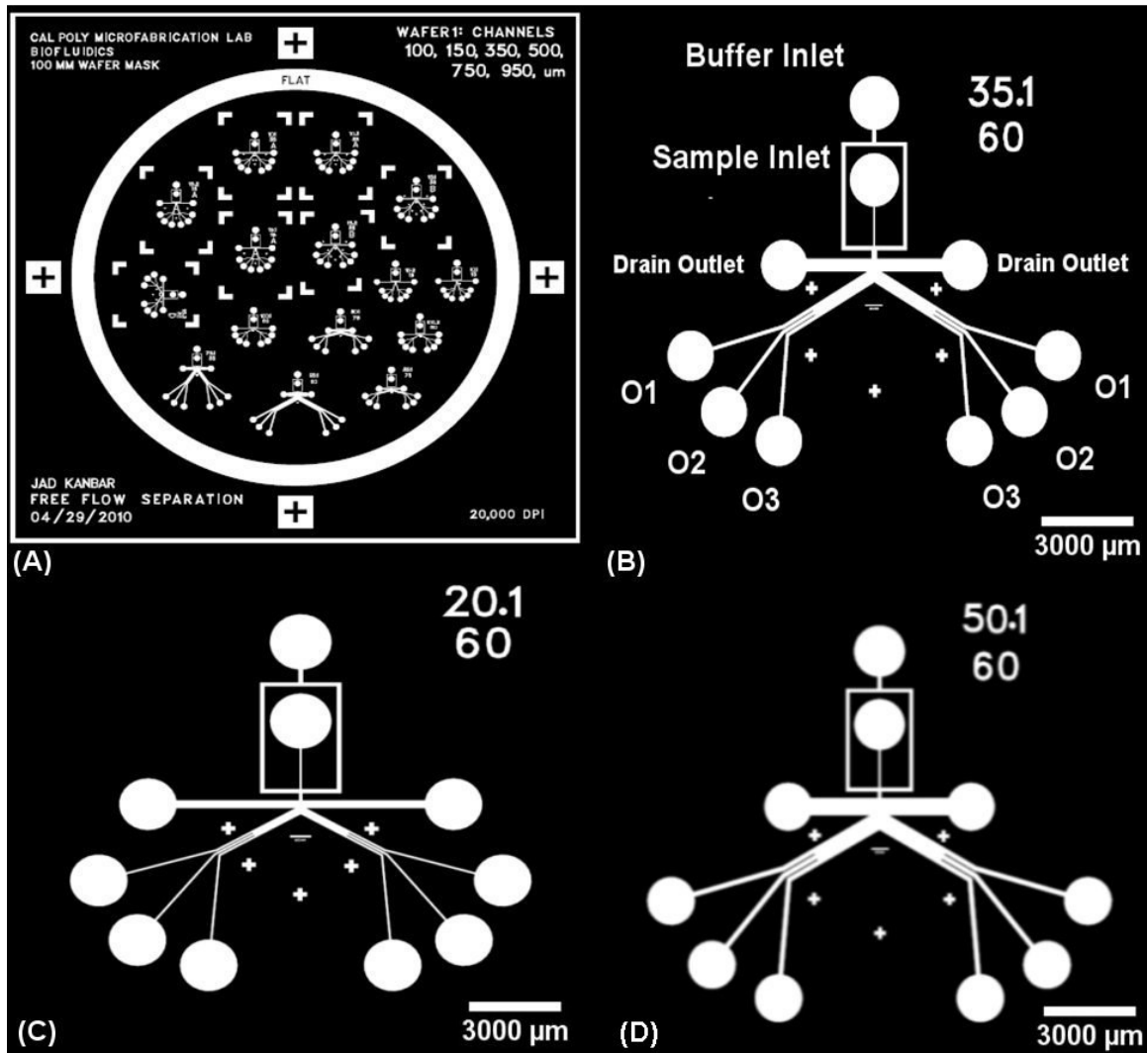
Figure 5. Transparency Mask and Device used in Fabrication.

(A) This is an image of a transparency mask used in fabrication. The dark circular region is placed over the wafer. Seven devices of varying geometry are shown in this mask. (B) This is an expanded view of one of the devices. All inlets and outlets are labeled; see text below for explanation of device labeling nomenclature. (C) A drawing of the same device from (B), but with collection outlet width of 200 µm. (D) A drawing of the same device from (B), but with collection outlet width of 500 µm.

As shown in Figure 5A, to save space, multiple devices were fit on one wafer mask, while leaving enough space between devices. All the inlet and outlet reservoirs were drawn to 1500 µm in diameter. The entire device is symmetric. Initially, it was unknown whether different sized devices and therefore Collection Outlets widths would have an effect on downstream separation of particles. To account for this, different devices were designed and tested.

Figure 5B-D shows the same device with identical channel lengths, but different Collection Outlet Widths – 200, 350, and 500 µm. A labeling system was used for easy device identification. Two numbers helped identify the device, one for outlet channel width and one for the collection outlet angle. For example, in Figure 2B top corner, '35.1' is short for a 350 µm outlet channel width and 1st design iteration for this specific device. The '60' in the top corner of Figure 2B designates the collection outlet angle, +/- from the negative y-axis of symmetry through the middle of the device.

Having finished drawing all the devices, the AutoCAD file was sent to CAD/Art Services, Inc. There, the file was printed on transparency mask at a resolution of 20, 000 DPI. It is important to specify the side to which the ink prints on the transparency because the side with ink later comes into contact with the photoresist in fabrication of the devices. Stating emulsion side down essentially prints the CAD file backwards so that when the transparency is flipped and viewed from above, the devices will be exposed and seen exactly as drawn. Once the transparency was received, the fabrication process of Soft Lithography was then carried out in the Cal Poly Clean Room.

2.2. Device Fabrication

2.2.1 Soft Lithography

Soft Lithography as a means of fabricating microfluidic chips can be traced back to one paper by the Whitesides group [3]. As shown in Figure 6, the overall processing steps are largely not labor intensive and thus it is possible to change design parameters without a great deal of lost time.
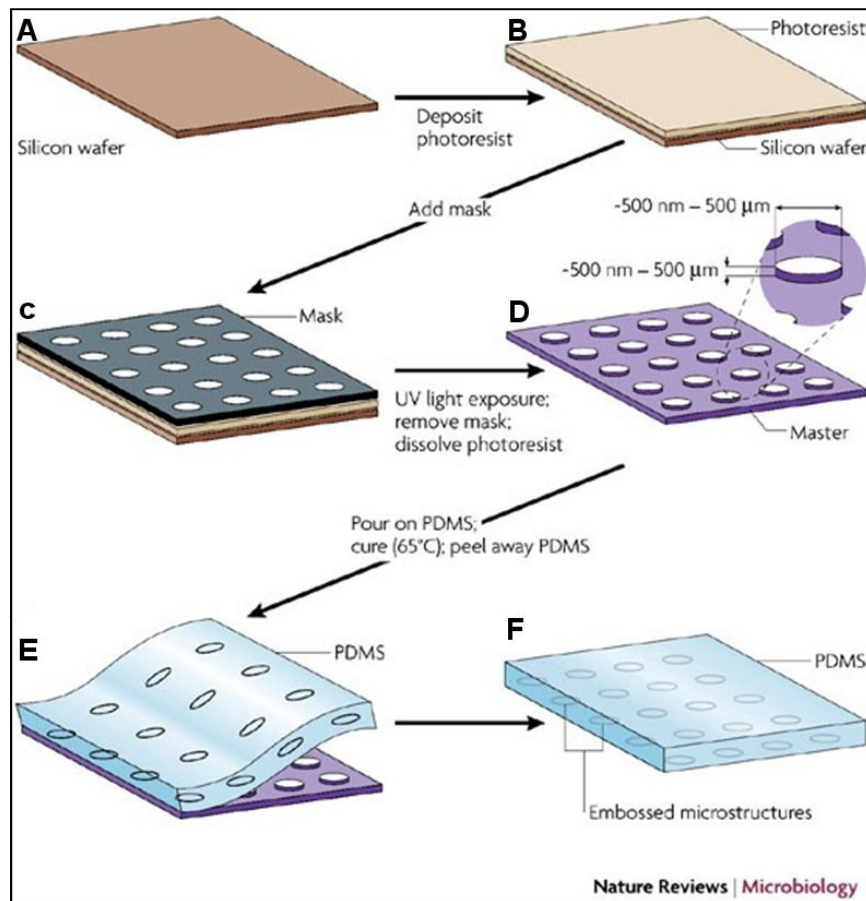
Figure 6. The overall process steps of soft lithography.

In the schematic above, the process steps are as follows: (A) A silicon wafer is cleaned, (B) photoresist is deposited on the wafer, (C) A transparency mask is brought into contact with the wafer and resist, (D) the resists is exposed to UV light and developed creating a master mold, (E) a PDMS polymer is cast over the mold and cured with heat, (F) the slab of PDMS is peeled off the mold and is ready for bonding to a substrate surface [25].

Perhaps the most time consuming aspect is the creation of a CAD drawing for photolithography, also the first step of soft-lithography. The second step involves the choice of a photoresist. In microfluidics a well characterized choice is an SU-8 negative photoresist, a photopolymer that hardens after exposure to UV-light [25]. Those regions not exposed to UV-light are soluble in developer. As shown in Figure 7, the regions exposed to UV-light will harden and become insoluble to developer.
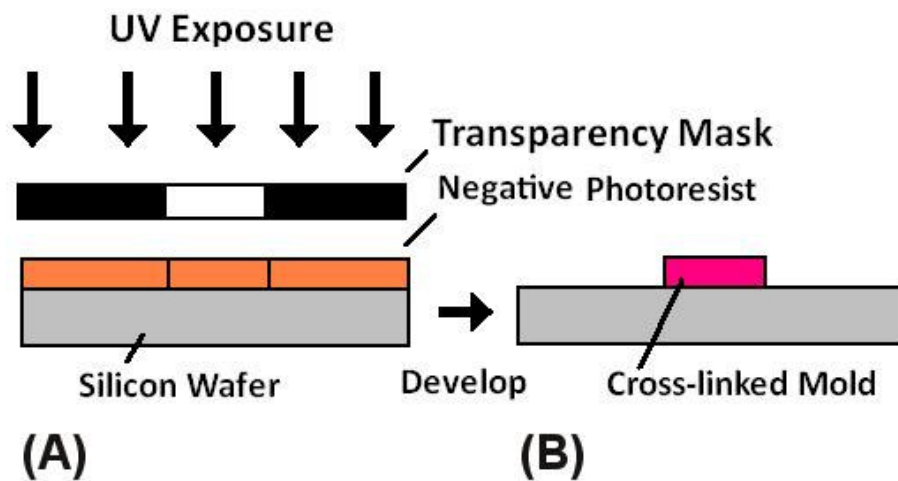
Figure 7. A schematic demonstrating how SU- 8 negative photoresist works.

(A) UV light is exposed from above a transparency mask. The region that is clear, shown in white, allows the UV light to shine through on to the layer of photoresist over a silicon wafer. This allows the exposed region to cross-link after heating, becoming insoluble to a developer. (B) The regions of SU-8 not exposed to UV light are soluble in developer; those regions exposed are not soluble and stay as a cross-linked mold.

Spin coating is used to deposit a film of photoresist unto a silicon substrate to a desired thickness. Soft Baking after spin coating aims to evaporate excess solvent prior to exposure. The baking time for this step is recommended by the photoresist manufacturer. The exposure dose depends on the photoresist used and desired thickness of features. Usually as a standard procedure, an exposure matrix is performed in order to fine tune

proper exposure doses needed to create the desired channel feature sizes. After exposure a post exposure bake initiates a reaction between the novolak epoxy resin and photoacid generator in the SU-8, forming the pattern that was exposed to U.V. light [26, 27]. The baking time for this step is also recommended by the photoresist manufacturer, but may be increased to allow the reaction to fully complete. The photoresist is then developed in solvent which may be supplied by the manufacturer or can be done in ethyl lactate [27]. The time in developer depends on the feature thickness.

After the lithographic fabrication steps, a master mold has been created and a polymer can be mixed for casting (see Figure 3). An elastomeric stamp, mold, or mask on its surface is the key element of soft lithography [26]. The most widely used polymer for channel molds is poly(dimethylsiloxane) (PDMS). The curing agent's silicon hydride group reacts with the vinyl group present of the base forming a cross linked elastomer [28]. The PDMS is cast over the master and cured in a heated oven creating a replica of the channels. The last general step involves sealing the PDMS slab to a surface. PDMS has been shown to irreversibly bind to itself, glass, silicon, silicon dioxide, quartz, silicon nitride [29].

2.2.2 Cleaning the Silicon Wafer

A <1-0-0> 4" P/B single side polished Silicon Wafer from Silicon Quest International, Inc. was loaded into a Teflon cassette and cleaned in Piranha (9:1 $H_2SO_4:H_2O_2$) at 70ºC for 30 minutes, then quenched in DI water. This was followed by 15 minutes in Buffered Oxide Etch (6:1 40% NH_4F:49%), then quenched in DI water.

The wafer was then dehydrated on a hot plate for 15 minutes at 150°C, and then cooled on a chill plate for 5 minutes.

2.2.3 Spin Coating of SU-8 2050

The bottle of SU- 2050 was taken out of the refrigerator 24 hours prior to fabrication. This allowed the photoresist to slowly reach room temperature to decrease its viscosity. Spin coating was done to create a uniform layer of resist that was later used as a mold for microfluidic chips. The inside of the spin coater, MODEL WS-400-8N/L as shown in Figure 8, was first covered with aluminum foil in order to prevent resist from sticking to the spin coater. The desired spin cycle was programmed to create the targeted thickness. There are two steps to the program, a spread cycle and spin cycle. The spread cycle aims to spread the photoresist across the wafer and was set for 20 seconds at 500 rpm, and acceleration of 172 rpm/sec. The spin cycle, the following step, is a longer spin and at higher revolutions in order to flatten the photoresist to the target depth.

To arrive at the required spin needed, the following equation was used [30]:

$$\omega = 0.9 \left(\frac{3}{4} v \right)^{1/2} h^{-1} \, t^{-1/2} \cdot \frac{60}{2\pi} \tag{27}$$

where ω is the rpm for the spin step, v is the kinematic viscosity of SU-8 2050, h is the target height, and t duration of the spin step. A factor of 0.9 was introduced to equation (27) to account for the non-Newtonian characteristics of SU-8 2050. The target height was 25 µm and spin time was set at 50 seconds. This gave a spin step of 4782 rpm for 50 seconds at an acceleration of 860 rpm.

The wafer was centered on the spin coater chuck using the centering ring shown in Figure 8, in front of the spin coater. The centering ring centered the wafer on the spin coater chuck and the "vacuum" button was pressed to create 25.5 psi of negative pressure holding the wafer down. A little strip of tape was placed along the major flat to allow a pair of tongs to hold onto the wafer cleanly. SU-8 2050 was then poured directly from the bottle on to the wafer. The amount of resist needed is usually the size of a half dollar coin in diameter. A wipe with acetone was prepared to catch dripping or excess resist from the bottle's lip after pouring. Once this was done, the program started and spun through the two steps as detailed. When the program ended, an edge-bead was usually present around the wafer as result of spin coating. This edge-bead is a ridge of photoresist around the circumference of the wafer. To get rid of this, a wipe with acetone was slowly pressed around the wafer edge to remove it. After spin coating, a soft bake step was performed.

Figure 8. The spin coater used for negative photoresist and centering ring.

2.2.4 Soft Bake

Soft bake is an important step before exposure. It helps drive out the solvent in the resist, which allows the features to be accurately exposed during exposure. The recommended temperatures and time on the hot plates were carried out at 55ºC for 10 minutes and 85ºC for 20 minutes on adjacent hot plates. The wafer was then cooled down on a chill plate for 2 minutes. After soft baking, exposure of the photoresist followed.

2.2.5 Exposure of Photoresist

Exposure was done using an aligner (Canon PLA – 501FA) shown in Figure 9. For exposure, the wafer was set up like a sandwich in the following order starting from the bottom up: a glass slide with marks to center the wafer, then 5 circular pieces of wipe (2" diameter) in the center, then the wafer with SU-8 side up, then glass slide with transparency mask facing down. Tape was used around the four edges to hold the two glass sides, sandwiching the wafer, and then loaded into the aligner. An Omega Filter, was used to eliminate UV radiation below 350 nm, and placed on top of the sandwiched components.

Figure 9. The alignerused for exposure.

Using energy related to the desired thickness provided by MicroChem [31] and the known aligner power of 1.03 mJ/(cm^{2}s), the exposure time was calculate. For a 25 µm thick resist layer, this time was found to be around 147 seconds. When the exposure was finished, the tape was cut around the edges, and the sandwich carefully pealed apart. A Post Exposure Bake followed.

2.2.6 Post Exposure Bake (PEB)

Post exposure bake is necessary to set the resist and help the exposed resist create cross-linking. The parts of the photoresist exposed to the UV radiation, determined by the transparency mask, are subject to cross-linking. The wafer was placed onto the hot plate set at 55ºC for 10 minutes and then moved onto another hot plate set at 85ºC for 20

minutes. The hot plate was then turned off, allowing the wafer to cool to room temperature. During PEB, the outline of the channels molds becomes apparent in the photoresist. The photoresist was then ready to be developed.

2.2.7 SU-8 Developer

This step removes uncross-linked SU-8 from the wafer. SU-8 developer was poured in a glass Petridish and the wafer was gently placed into the dish for 5 minutes. Slight periodic agitation was done to speed up the developing. After 5 minutes, Isopropyl alcohol was sprayed over the wafer as a test to see if the developing had completed. If a milky white residue appeared, this meant that the photoresist had not fully developed and additional developing was needed, usually at increments of 5 minutes at a time. Afterwards the wafer was taken out the Petri dish, rinsed with DI water, dried with low purity Nitrogen gas, and observed under a light microscope as seen in Figure 10.
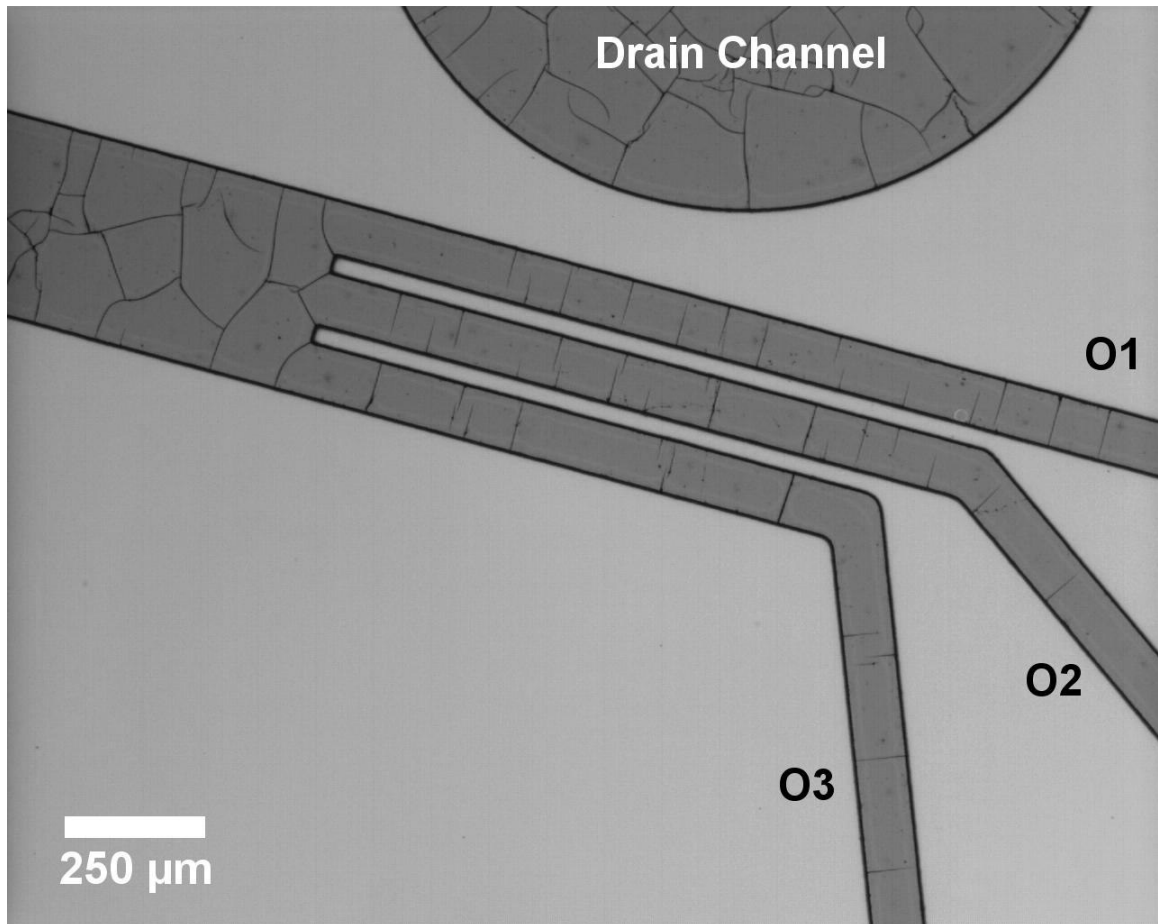
Figure 10. SU-8 mold of a device after developing.

This an image taken at 10X of a wafer with an SU-8 mold after developing. The device features are all fully resolved and the channels imaged are al labeled. Cracks are seen in the SU-8 mold indicating a Hard Bake step is required.

2.2.8 Hard Bake

Hard baking the wafer in this case aims to remove cracks in the SU-8 mold after processing and developing. The wafer was placed on a hot plate at 200ºC for 30 minutes, allowing the SU-8 mold to cure and 'heal' its cracks. Following this, the wafer was cooled for 5 minutes on a chill plate and devices were observed under a light microscope as seen in Figure 11. The SU-8 mold was then ready for its purpose of creating microfluidic devices using PDMS.
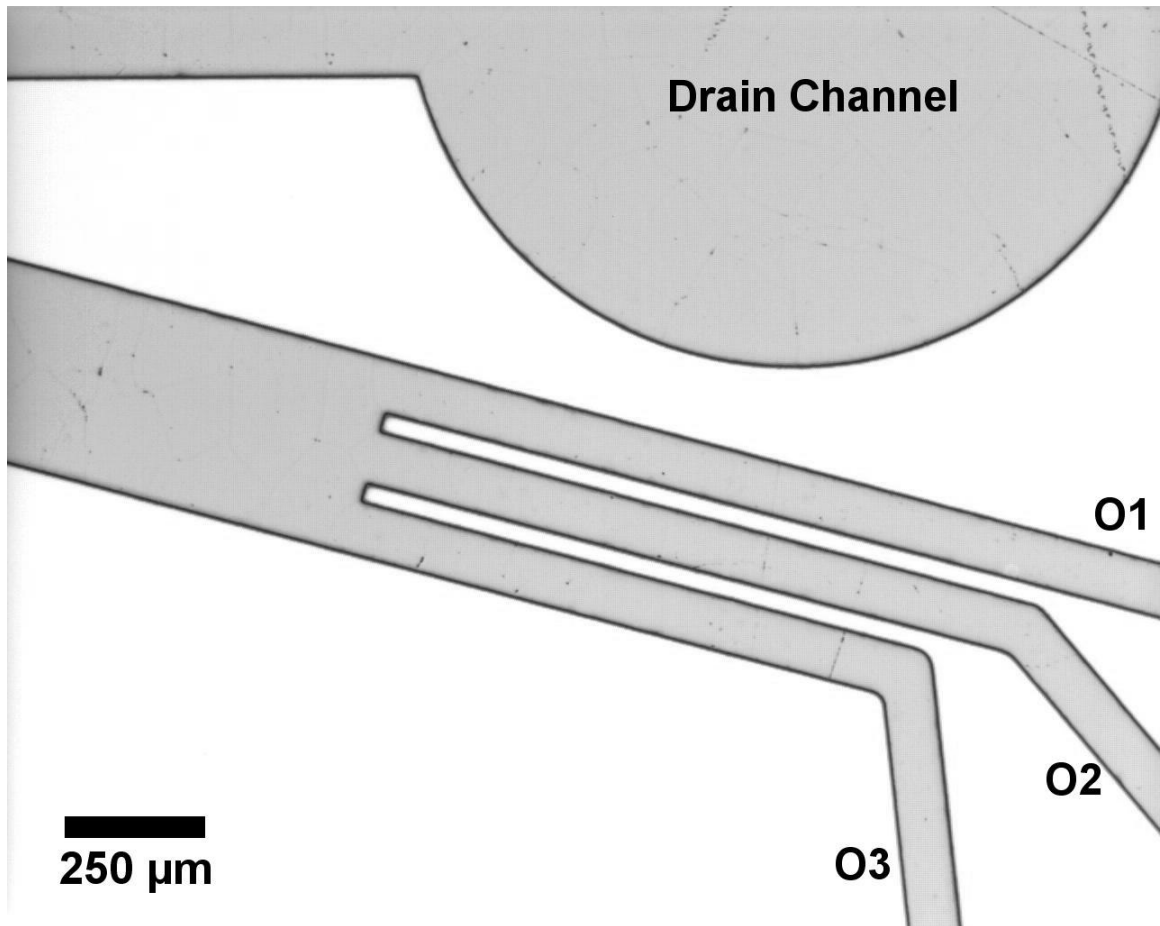
Figure 11. SU-8 mold of a device after hard baking.

This an image taken at 10X of a wafer with an SU-8 mold after developing. This device is the same one taken in Figure 10. The device features still remained fully resolved and the channels imaged are all labeled. Cracks that were presently in the SU-8 mold after developing were for the most part cleared. Surface scratches on the SU-8 mold are observed due to prior contact with the transparency during the exposure step.

2.2.9 Choosing the Casting Material

The most widely used polymer for channel molds soft lithography is poly(dimethylsiloxane) (PDMS) [10]. PDMS formulations are made of two components; pre-polymer or curing agent, with viscosity of $0.0050 m^2/s$, and a cross linker or base, with viscosity of $0.0011 m^2/s$ [32]. The cross-linker has a smaller viscosity than pre-polymer. The curing agent's silicon hydride group reacts with the vinyl group present on

the base, forming a cross linked elastomer [28]. Heat speeds up this reaction process. Increasing amounts of cross-linker relative to the curing agent to form the different formulations, leads to a reduced effective viscosity.

After mixing, PDMS is cast over a master mold creating a replica of the channels and thus creating a microfluidic device. It is a useful material because PDMS is generally inexpensive, flexible, and optically transparent down to 230 nm and therefore compatible with optical methods for detection [33]. It is also biocompatible and highly permeable to CO_2 and O_2 allowing for biological assays and cell culturing experiments [6]. Oxidation of PDMS channels can create high surface energy allowing polar liquids like water to easily fill the channel [27]. The negative surface charges caused by oxidation can also support electro-osmotic flow toward the cathode [27].

However PDMS does pose some disadvantages. It can swell or dissolve in many nonpolar organic solvents [4, 5, 35]. This can cause PDMS to deseal from the glass it is bonded to. Since glass does not swell from these solvents, the swelled PDMS comes under stress and the stress is relieved by desealing from the glass [34]. Also, since PDMS is elastomeric, at feature sizes with an aspect ratio greater than 10 to 1, it can sag if support posts are not included in the design. Lastly, it is not a very durable material and cannot endure repeated use effectively.

2.2.10 Mixing Formulations of PDMS

PDMS (Sylgard 184) was used to create the channels for the microfluidic devices used in this project.A shown in Figure 12, the two components of PDMS, Base and Curing Agent are mixed in a 10:1 ratio, and then cross-linked through in an oven with

heat. The typical ratio of volumes used in the project ranged anywhere from 50:5 to 20:2 in mL. A 30 mL syringe removed the exact volume of Base and a 3 mL syringe removed the exact volume of Curing Agent, into a plastic cup. A stir rod was then used to vigorously mix the two components which created air bubbles that required a vacuum for removal.
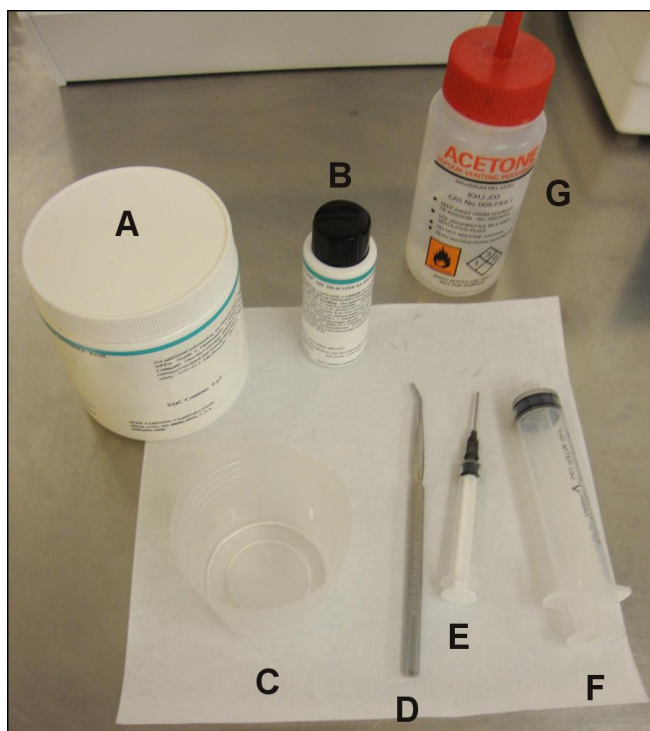
Figure 12. All the materials and tools needed to mix formulations of PDMS.

The following components are as follows: (A) Sylgard 184 Base, (B) Sylgard 184 Curing Agent, (C) a plastic cup, (D) a metal stir rod, (E) a 3 mL syringe used for the Curing Agent, and (F) a 30 mL syringe used for the Base, and (G) acetone used to clean PDMS from the tools and lab bench.

The cup was placed into a vacuum chamber as showing in Figure 13, to degas the PDMS mix at pressure around -27 in Hg. The vacuum was controlled with a check valve so that the bubbles did not expand over the top of the cup, but balanced so as continue the

removal of air bubbles from the PDMS mixture. Degassing was completed when all the air bubbles were gone.

Figure 13. The vacuum chamber used to degas the PDMS mixture.

The PDMS mixture was then poured onto master silicon mold, placed in a Petri dish. Pouring was done as close as close to the wafer without touching, to prevent air from entering the PDMS again. Once most of the PDMS was poured into the Petri dish, the PDMS was cured in an oven at 70ºC for at least 1 hour. As shown in Figure 14, after curing the devices could then cut out from the wafer directly and prepared for bonding and subsequent use.
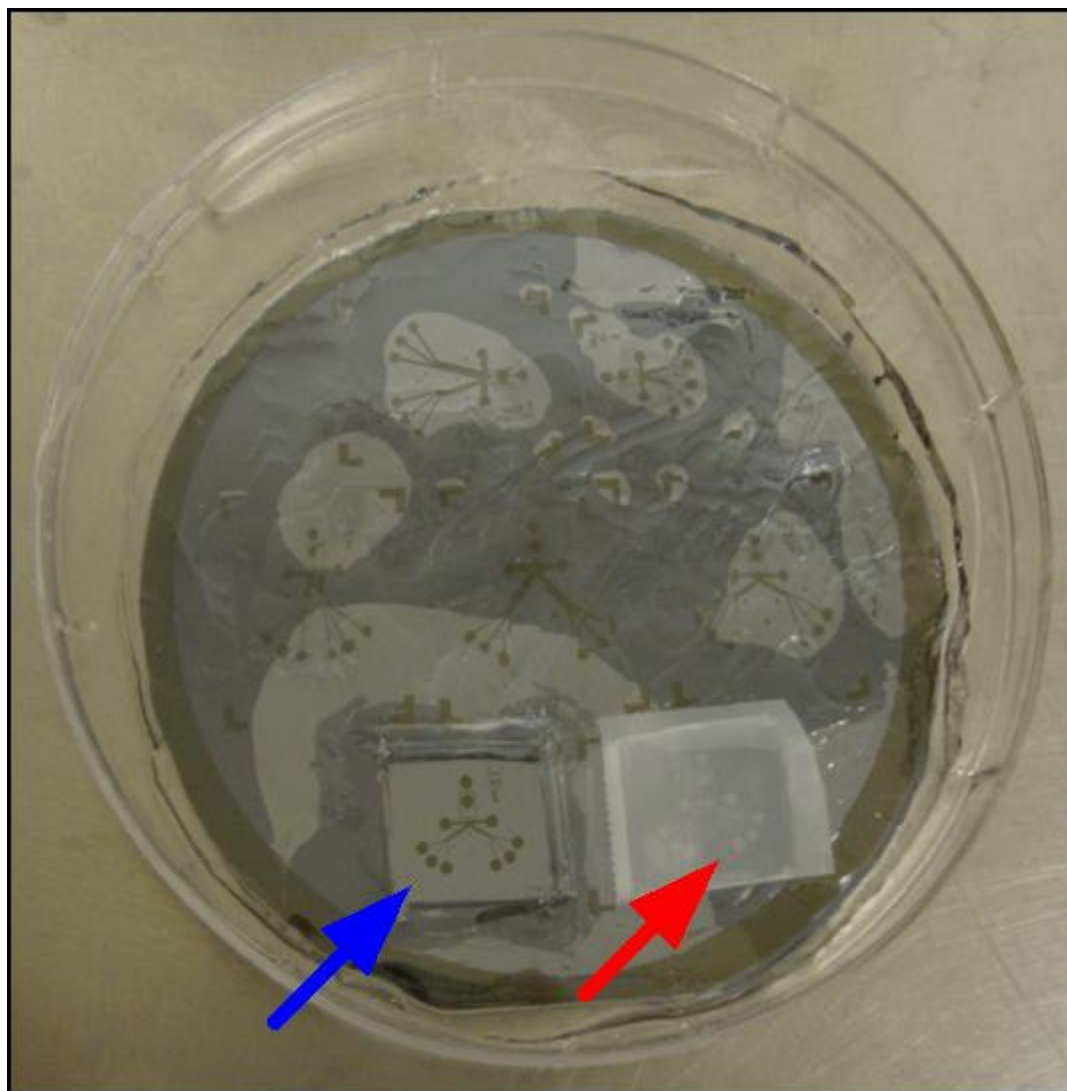
Figure 14. A Silicon wafer with SU-8 mold placed inside a Petri dish and PDMS layer cured on top.

In this image, the wafer has finished the entire soft lithography process and has the same microfluidic designs from the transparency mask as seen in Figure 5. The blue arrow indicates a device that has been cut out from the layer of PDMS. The red arrow indicates this device facing up with tape covering the channels preventing contamination from dirt.

2.2.11 Inlet hole punching

The device cut out from Figure 14 is shown in Figure 15. Holes had to be punched through the top of PDMS to create connections to the channels. Red dots were

placed on tape which covered the microfluidic channels. For all Buffer Inlet connections,

Drain Outlets, and Collection Outlets, a 16 gauge beveled blunt tip needle was used. The

needle from above was lined up with the red dot below, and punched through PDMS.

Accuracy of hole-punching was not an issue after several practice runs.
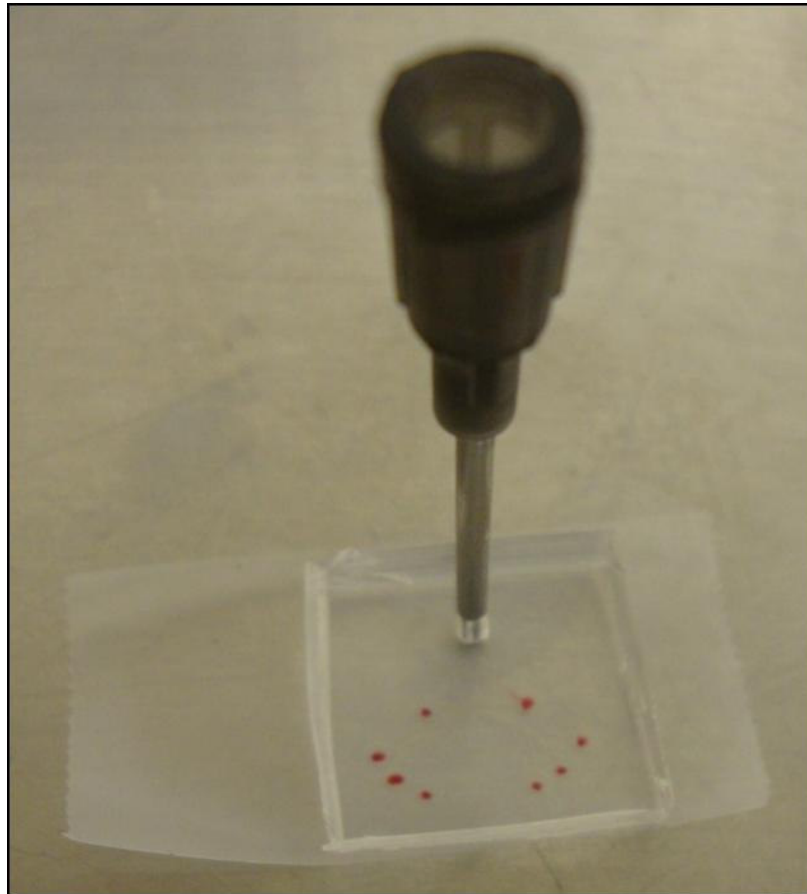
Figure 15. A device in the process of hole punching.

This is the device cut out from Figure 14. Red dots are seen on the tape placed below and over the channels to indicate the location for channel connection. A 16 gauge beveled blunt tip needle is shown punching through the top of the PDMS at the Buffer Inlet site.

The tools necessary for hole-punching are show in Figure 16. It was important

that the tape stayed over the channels throughout the hole-punching and bonding

processes in order to keep them clean of dirt particles.
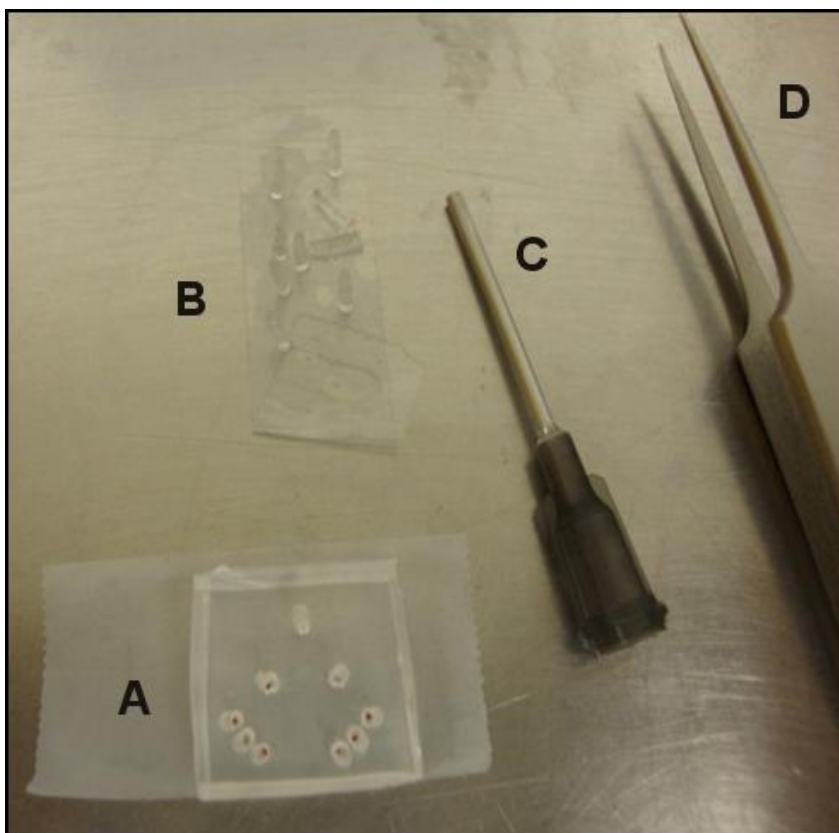
Figure 16. A display of all the tools needed in the hole punching process.

The components above are as follows: (A) The device from Figure 15, with complete punched inlets. Tape still remains underneath covering the channels. (B) Double sided tape with the "mini-barrels" of PDMS removed from the hole-punching. (C) A 16 gauge, beveled blunt tip needle used to punch the holes. (D) Tweezers that were used to pick out the mini-barrels of PDMS from the device.

The inlet connections punched into the sample reservoir varied in diameter based on the gauge of needle used. In this project, varying the diameter of the inlet connection to the sample inlet reservoir was a very important experimental parameter. The three different gauge needle sizes used were a 23 gauge, a 20 gauge, and an 18 gauge as seen in Figure 17. The relative position of the hole-punch inside the sample inlet reservoir was varied, from the top of the reservoir, to the middle and bottom. After hole-punching was completed, the chips were ready for bonding to a glass slide.
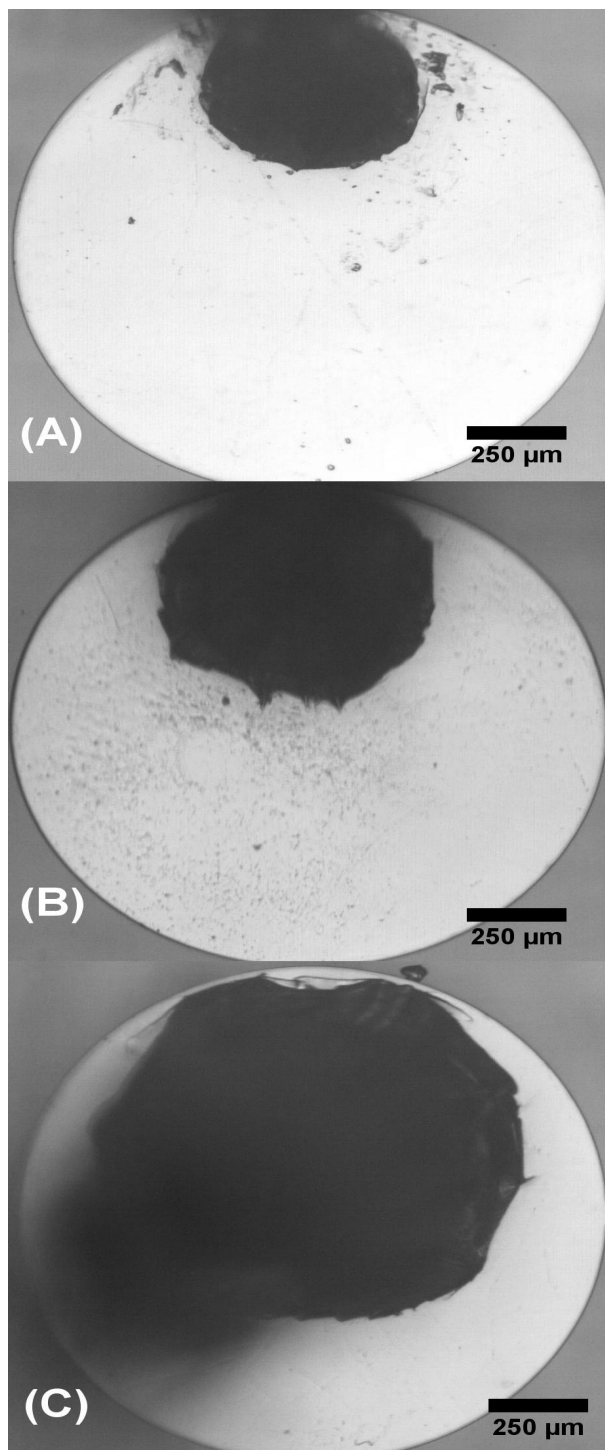
Figure 17. A stack of images showing the different inlet hole sizes.

The punched inlet is seen as black shadow inside the white background of the sample inlet reservoir. (A) A sample inlet hole created using a 23 gauge, (B) a 20 gauge, and (C) an 18 gauge beveled blunt tip needle.

2.2.12 Plasma bonding of Chips

To bond the microfluidic chips to a glass slide, a Duradyne, Tri-star Technolgies plasma machine was used, as shown in Figure 18. Argon gas was first turned on to generate the plasma and the machine was set to 70% of 25 watts. Just before plasma bonding, a 3 x 1 inch glass slide was cleaned with Isopropyl alcohol using a kimwipe to increase adhesion. Tape that had covered the channels was also removed. Once turned on, the plasma gun was placed roughly 3 inches off of the surfaces. Plasma treatment was first guided over the glass bonding region, then on to the PDMS surface. The rate of treatment was slow, roughly 8 to 10 seconds per inch, and the motion followed a rastered profile.

Only after both surfaces were treated was the plasma turned off. Immediately after plasma treatment, the PDMS device was carefully picked up around its edges, making sure to not touch the channel surface, flipped and dropped less than a half inch away from the glass slide. This was to ensure that air between the PDMS and glass surface would be pushed out, leaving no air bubble in between. An air bubble over a channel would compromise the entire device. If it looked like there was an air gap, light pressure was applied to the top surface of the PDMS, forcing contact. Too much pressure however and a channel could be pushed and collapsed to the glass. Once the PDMS was in contact with the glass surface, it was instantaneously and irreversibly bonded. Two PDMS devices were bonded per glass slide, and an example is shown in Figure 19.

Figure 18. A picture of the plasma bonder and gun used to bond the PDMS devices to glass.
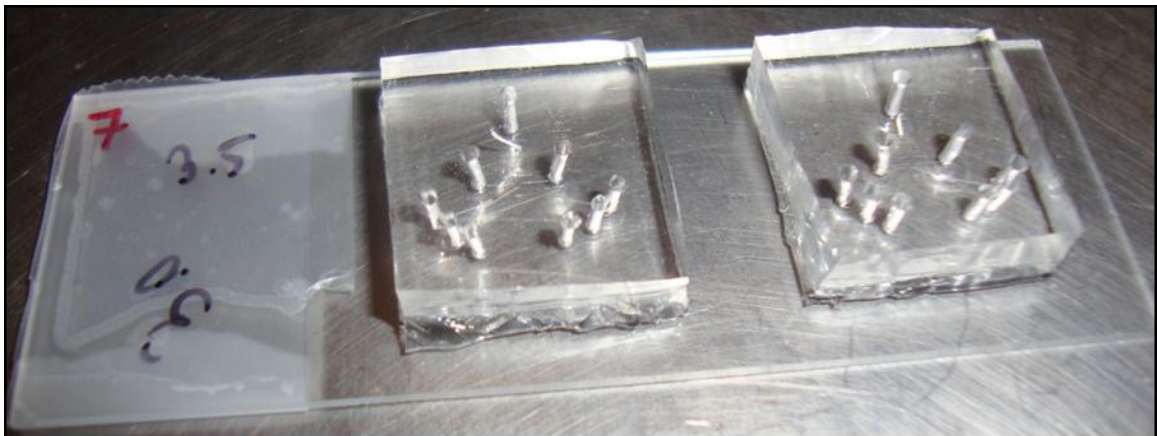
Figure 19. A picture of two microfluidic devices bonded to a 3 x 1 inch glass slide.

2.3 Experimentation

2.3.1 Fluorescent Microspheres

Initially a diluted solution of Tween 20 was prepared at 0.045% v/v concentration. 450 µL of Tween 20 was diluted into a 10 mL of DI water. 1ml of 0.045% Tween 20 was then pipetted into a 1.5 ml microcentrifuge tube. The fluorescent microspheres where then diluted into this microcentrifuge tube. No cleaning of the spheres was carried out because the sample volumes taken from the stock solution were so low that it was deemed unnecessary. Four different types of microspheres were used in this project as listed in Table 4.

Table 4. List of all Fluorescent Microspheres Used in Experiments

Company	Color	Diameter of Microspheres (µm)	Excitation/Emission (nm)
Invitrogen	Red	10	580/605
Spherotech	Yellow High Intensity	5.5	450/475
Spherotech	Nile Blue	3.0	615/640
Invitrogen	Nile Red	1.1	535/575

The number of microspheres/mL was determined by using the following equation [35]:

$$\frac{6C \times 10^{12}}{\rho \times \pi \times \emptyset^3} \tag{28}$$

where C is the concentration of suspended beads in g/mL, Ø is the diameter of microspheres in µm, and ρ is the density of the polystyrene beads (1.05 g/mL). Table 5 lists the dilutions from equation (28) used during experimentation.

Table 5. List of Microsphere Concentrations Used in all Experiments

Diameter of Microspheres (µm)	Concentration of Suspended Beads (g/ml)	Number of Stock Particles (microspheres/mL)	Volume of Stock Used (µL)	Number of particles/µL
10	0.002	3.6×10^6	298.8	2.1×10^5
5.5	0.005	5.5×10^7	7.7	2.1×10^5
3.0	0.01	6.7×10^9	0.31	2.1×10^5
1.1	0.02	2.7×10^{10}	0.004	2.1×10^5

In this project 10 µm, 5.5 µm, and 3.0 µm particles were mixed together during most experiments. Experiments using 1.1 µm particles were done alone and not mixed with other beads.

2.3.2 Syringes and Syringe Pumps

During experimental testing, only two Harvard Apparatus Model 11 Syringe pumps were used as shown in Figure 20. One syringe pump connected to the buffer inlet and was placed with a 1 mL BD Syringe filled with Rhodamine B at a concentration of 0.0023g/mL w/v. This fluorescent tracer dye was used to enhance the viewing of the hydrodynamic focusing profile. The flow rate used to the buffer inlet was set for 10 µL/hr and stayed constant in all experiments. The other syringe pump connected to sample inlet and was placed with a 1 mL BD Syringe filled with the microsphere dilutions (fluorescent beads in 0.045% Tween 20). The flow rate used to the sample inlet

was set for 5 µL/hr and stayed constant in all experiments. The inside diameter of both syringes in each pump was setto 4.78 mm.

Tygon tubing connecting to the buffer inlet was inserted directly into the chip without an interconnection because this inlet connection was punched with a 16 gauge needle. According to the experiment, different sized blunt tip needles, 23 gauge, 20 gauge, and 18 gauge, were clipped and sand-papered to smoothness, then inserted into the sample inlets with attached tygon tubing. If needed, tygon tubing of the same length, roughly 6 inches in length, was easily inserted to all outlet channels for waste and sample collection.

2.3.3 Video Microscope

All microfluidic chips bonded to a glass slide were placed over a Labsmith SVM340 Synchronized Video Microscope for experimentation as shown in Figure 20. Each experiment was performed under a 5x objective with a 1.5 x 1.5 mm field of view, 15.97 mm working distance, and 31.0 mm focal length. This objective allowed easy view of the collection outlets, the ability to focus to the channels, and different size particles could easily be distinguished. A Black and White Camera module was used as recommended by the manual for fluorescent experiments. The multi-color SVM340 illuminator used has 24 LED lights, separated to 1 blue, 1 green, 1 red, and 1 white channel. These different color channels allowed simultaneous excitation of all the particles in the experiments. A 630 nm long pass filter was placed underneath the 5x objective and thus underneath the illuminator lights. The overlap in excitation/emission spectra of the particles did not interfere with the fluorescence of the particles. This was a

curious result but helped experiments with mixes of three different fluorescent particle sizes, 10 µm, 5.5 µm, and 3.0 µm.
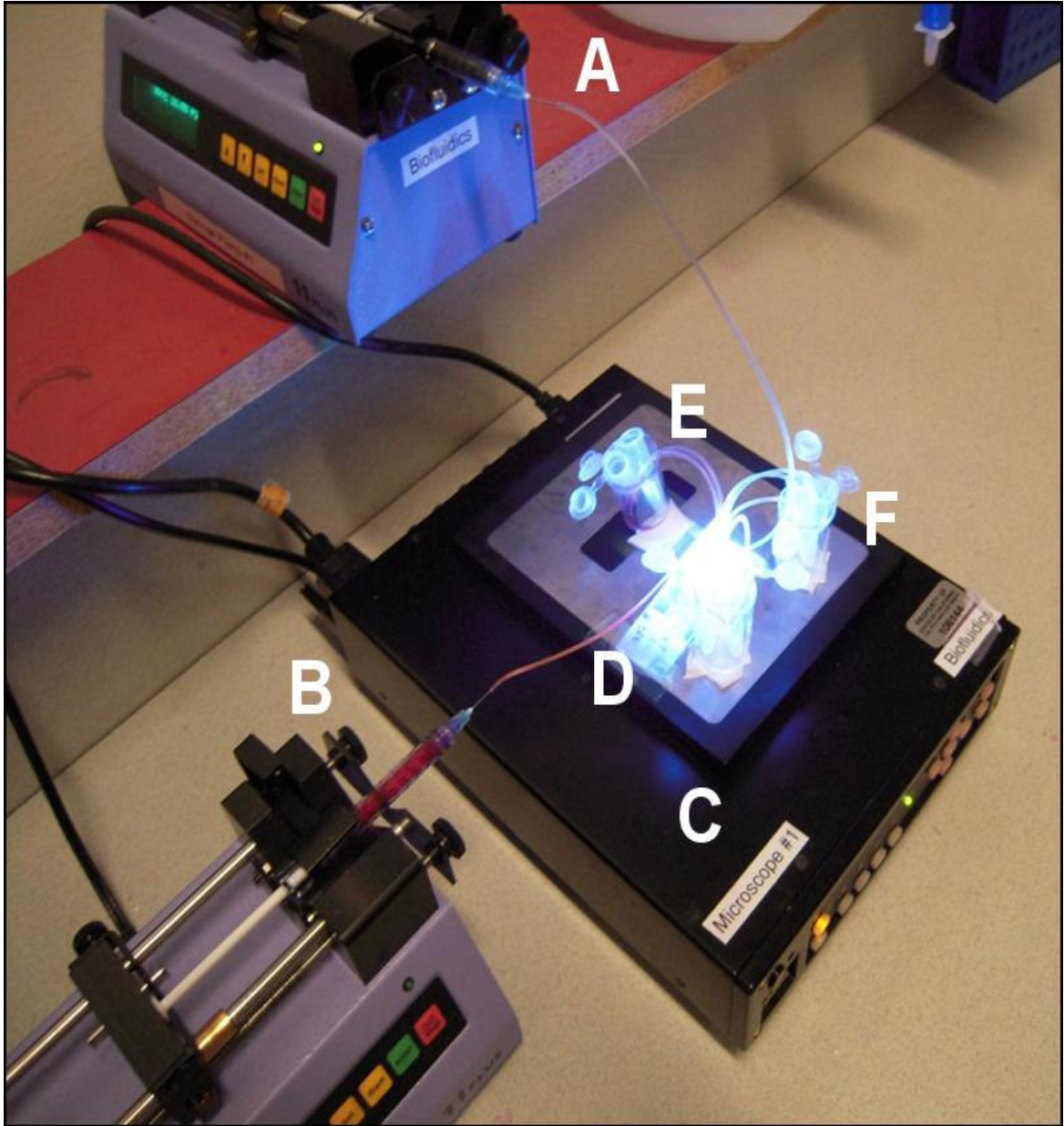
Figure 20. An image of the overall working test station used on all experiments.

The labeled parts above are as follows: (A) the Sample Inlet Pump and Syringe filled with microspheres, (B) the Buffer Inlet Pump and Syringe filled with Rhodamine B, (C) an SVM340 Video Microscope, (D) a glass slide with bonded microfluidic devices over an illuminated objective, (E) a beaker containing microcentrifuge tubes with tygon tubing running from the two drain channels, and (F) a beaker containing microcentrifuge tubes with tygon tubing running from collection outlets.
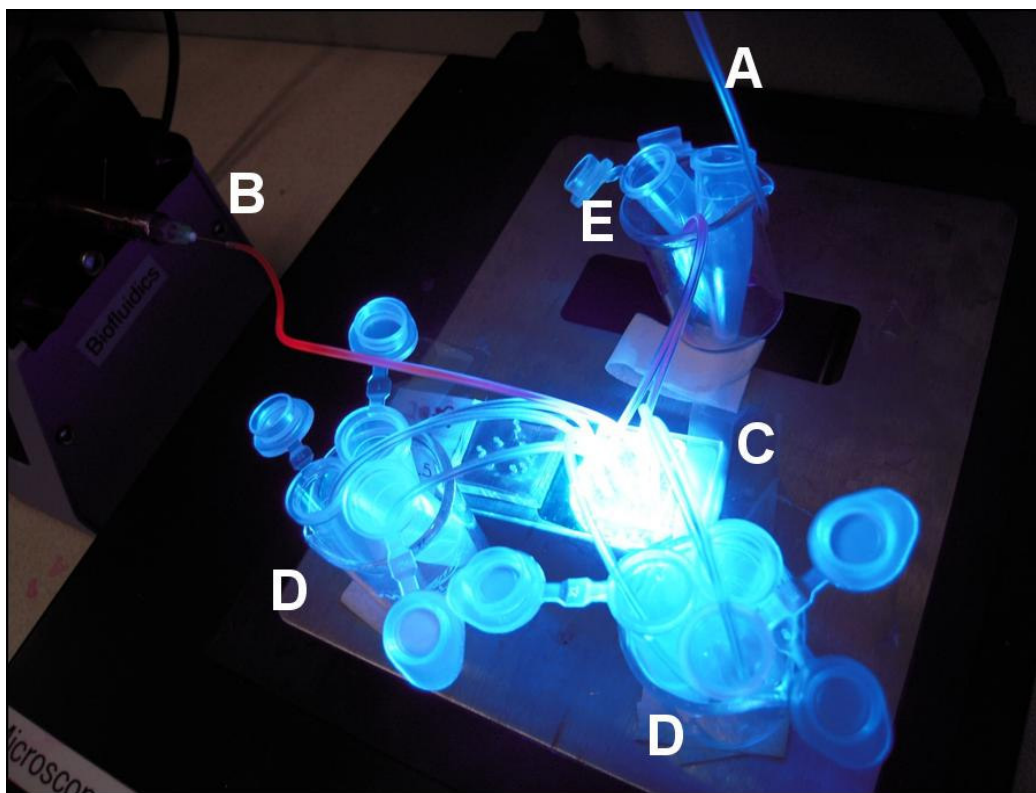
Figure 21. A close up image of a microfluidic chip in the process of an experiment.

This is the same chip as seen Figure 20. The labeled parts above are as follows: (A) Sample Inlet tubing with microspheres, (B) Buffer Inlet with Rhodamine B, (C) A glass slide with microfluidic chips, (D) beakers with microcentrifuge tubes containing tygon tubing attached to the Collection Outlets, and (E) a beaker with microcentrifuge tubes containing tygon tubing attached to the Drain Outlets.

2.3.4 Particle Microsphere Counting

Before running each experiment, the microfluidic chip made of PDMS was placed in a vacuum chamber for 15 to 20 minutes. Since PDMS is a material permeable to gas, air bubbles are prone to trapping in channels. These air bubbles cannot dissipate into the surrounding PDMS walls. Vacuuming out the air from the PDMS chip just before operation allows any air bubbles initially introduced during inlet connection to dissipate to the surround PDMS walls. Once tubing was attached to buffer and sample inlet, the

pumps began running. Videos were recorded as soon as the particles began to enter the chip through the sample inlet connection. These videos recorded particle movement at 30 frames per second. The field of view was generally placed at the point where the separation collection outlet split into three channels as shown in Figure 22. Each experiment ran for roughly 1 to 1.5 hours with continuous videos of 30 seconds to 1 minute clips. For a particular chip geometry and sample inlet diameter, the experiment was repeated two to three times on independent devices. This was to ensure reproducibility. After each experiment, videos of particle separation were analyzed by pure counting. As stated above, the flow rates used were slow enough that it was easy to distinguish each particle diameter and to which outlet channel a particular microsphere distributed to. In case of potential ambiguity for a specific video, the counting was repeated two to three times for an average. The results of counting from each video and was inputted into an excel sheet, an example is shown in Figure 23.
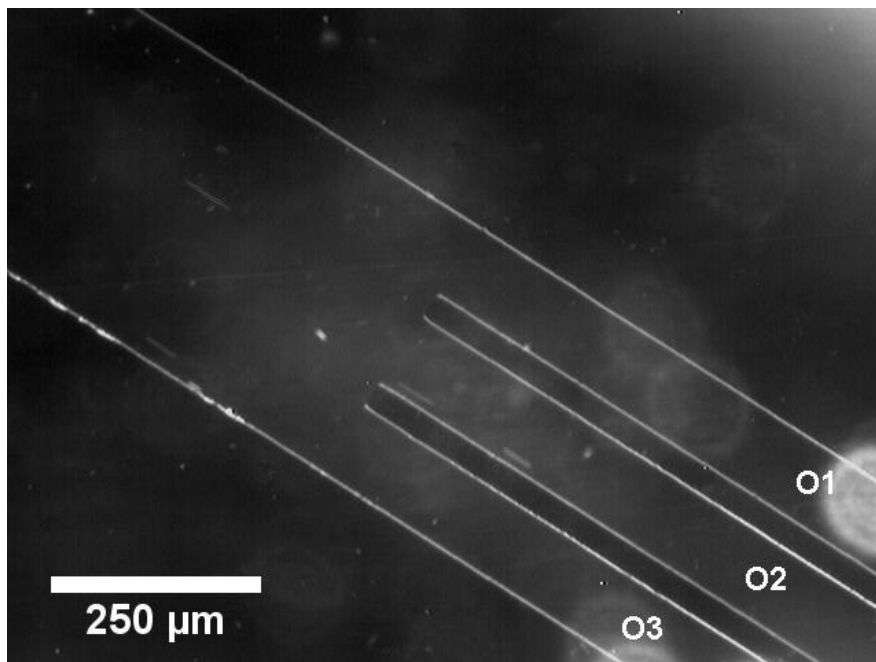
Figure 22. An image of the experimental separation viewing window.

48

Sample Inlet Diameter: 23 gauge | Inlet Position: Top | Chip Design and degree: 350 μm and 60 degrees | Experiment: 1

			Outlet 1				Outlet 2			Outlet 3		
Video	Time (sec)		10 μm	5.5 μm	3.0 μm	10 μm	5.5 μm	3.0 μm	10 μm	5.5 μm	3.0 μm	
301	94		11	9	11	21	23	10	8	4	10	
302	92		4	4	7	0	17	8	1	4	12	
303	36		5	2	2	18	11	5	4	4	8	
304	38		9	2	10	2	8	5	0	6	6	
305	55		17	2	7	2	11	4	1	6	4	
306	31		3	4	2	5	24	4	7	4	7	
307	60		17	11	12	5	6	2	5	6	5	
308	28		14	11	0	2	23	5	1	0	9	
309	35		4	13	0	8	8	5	5	7	6	
310	35		14	6	4	2	2	1	0	4	6	
311	41		17	2	6	6	9	3	1	6	3	
312	42		14	9	0	5	21	9	2	1	10	
313	45		30	0	0	2	8	11	1	8	11	
314	54		21	8	4	7	9	12	2	2	15	
315	30		17	8	30	3	2	3	0	0	5	
316	60		22	8	27	7	11	10	0	0	9	
380	60		15	6	10	6	13	10	2	2	14	
		Total	234	103	133	101	204	108	40	61	139	

Total Particle Distribution | Outlet1 | Outlet2 | Outlet3 | Total

			Outlet1	Outlet2	Outlet3	Total
		10 μm	234	101	40	375
		5.5 μm	103	204	61	369
		3.0 μm	133	108	139	380

Figure 23. A capture screen of an excel file with the data from an experiment.

49

III Results

3.1 Outlet Flow Rate

Initially the total flow rate distribution to the outlet channels of the fabricated device was compared to the theoretical design based on an equivalent circuit model. The theoretical model was designed such that 80% of the outlet flow rate would exit towards the drain channels, and 20% of the outlet flow rate would exit towards the six collection channels. The device was allowed to run at intervals of 30 minutes and sample volumes from each drain channel and collection outlet was pooled, and weighed.

As shown in Figure 24, the ratio of weight was compared in a w/w % and graphed. This experiment was repeated twice, using both a 2:1 and 3.2:1 inlet reservoir to inlet diameter ratio. No discernible differences between the ratios were observed and the experimental results closely matched that of the theoretical model.
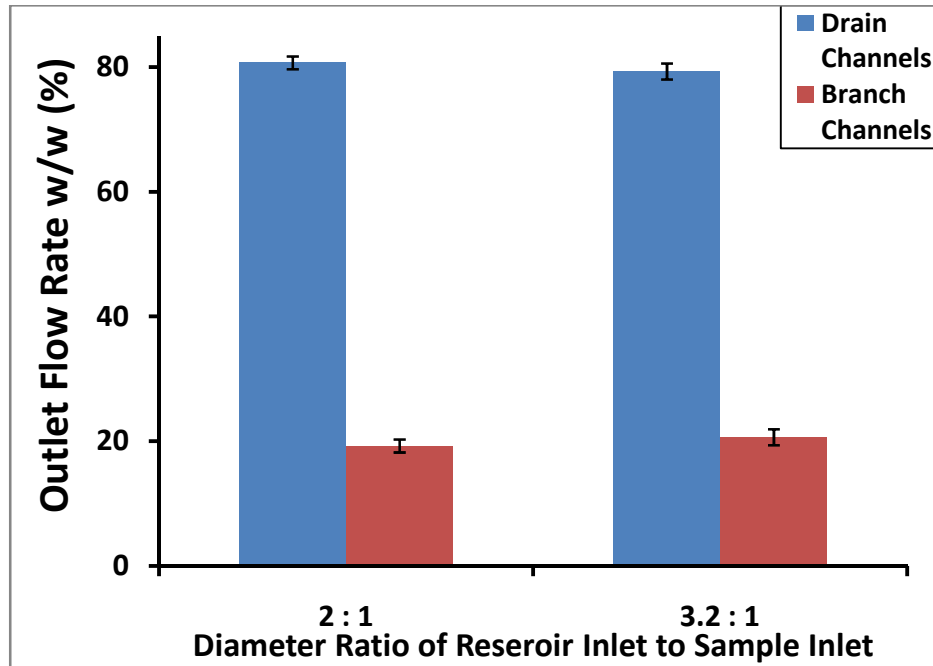
Figure 24. Flow rate ratios to the outlet reservoirs.

The Figure above shows the total flow rate exiting from the outlets of both drain channels and all collection channels. (A) In a 2:1 ratio the total flow rate out the drain outlets in was just below 80% and out the collection outlets just below 20%. (B) In a 3.2:1 ratio the total flow rate out the drain outlets in was just below 80% as well and out the collection outlets just below 20%.

3.2 Experimental Throughput

The relative throughput of the device for each particle was determined as a total rate summed from all six collection outlets and graphed in Figure 25. The total amount of particles exiting through the collection outlets per unit time was roughly the same for all particles. A decreasing rate with increasing particle size is observed, however the differences are within an acceptable range.
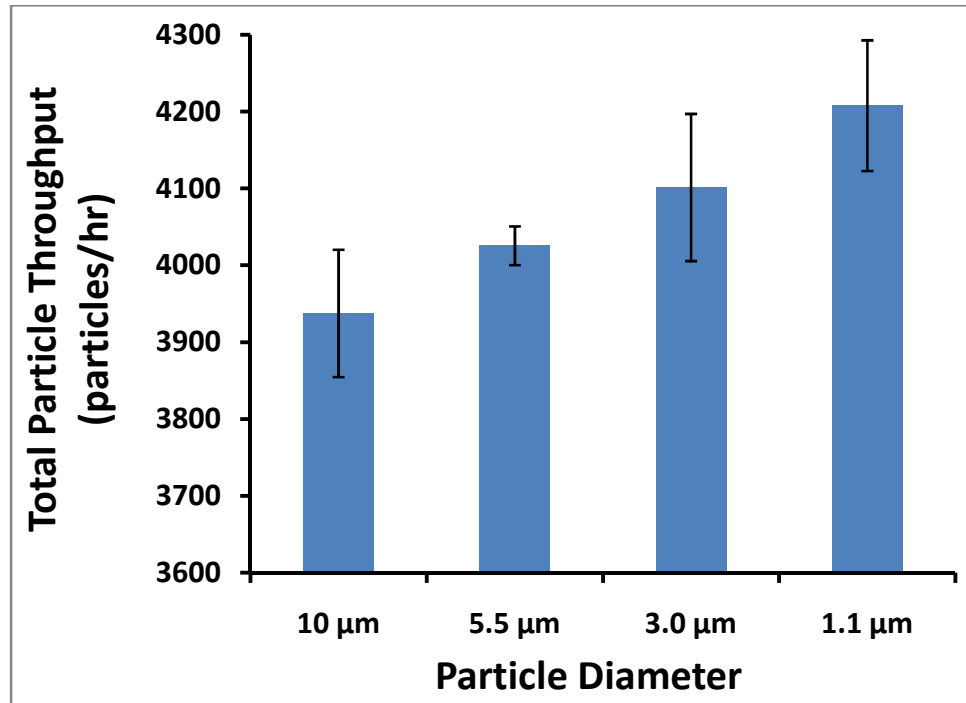
Figure 25. Total particle throughput of each particle from all collection outlets.

3.3 The Inlet Reservoir with Varying Sample Inlet Diameter

The inlet connections punched into the sample reservoir varied in diameter based on the gauge size of blunt needle used. The three different gauge needle sizes used were a 23 gauge, a 20 gauge, and an 18 gauge needle as shown previously in Figure 17. A ratio was used to describe the diameter of inlet reservoir relative to the punched inlet diameter. A 3.2:1 ratio corresponds to a 23 gauge hole-punch, a 2:1 ratio corresponds to 20 gauge hole-punch, and a 1.4:1 ratio corresponds to an 18 gauge hole-punch. Using COMSOL Multyphysics, the velocity profiles within the inlet reservoir of each inlet ratio was modeled. Figure 26 shows a of representative model device with arrows indicating the direction of flow. Sample inlets of the three different diameters were placed at the top of the reservoir, and the same experimental conditions, a sample inlet flow rate of 5 µl/hr

and buffer inlet flow rate of 10 µl/hr, were implemented as boundary conditions. Only the steady-state Stokes Flow module was utilized.

Different ratios resulted in different particle migration trajectories at the inlet reservoir; this is seen by both experimental observations and COMSOL models of the velocity streamline paths. Figure 27A- C shows that a 3.2:1 ratio created a particle trajectory that was more pinched and narrowed, with incomplete sampling of the entire inlet reservoir. Figure 27D- F shows that a 2:1 ratio created a particle trajectory that was wider allowing the particles to spread over the entire inlet reservoir. Lastly Figure 27G-I shows that a 1.4:1 ratio approached the channel exiting the reservoir and particles were not given enough space to spread.
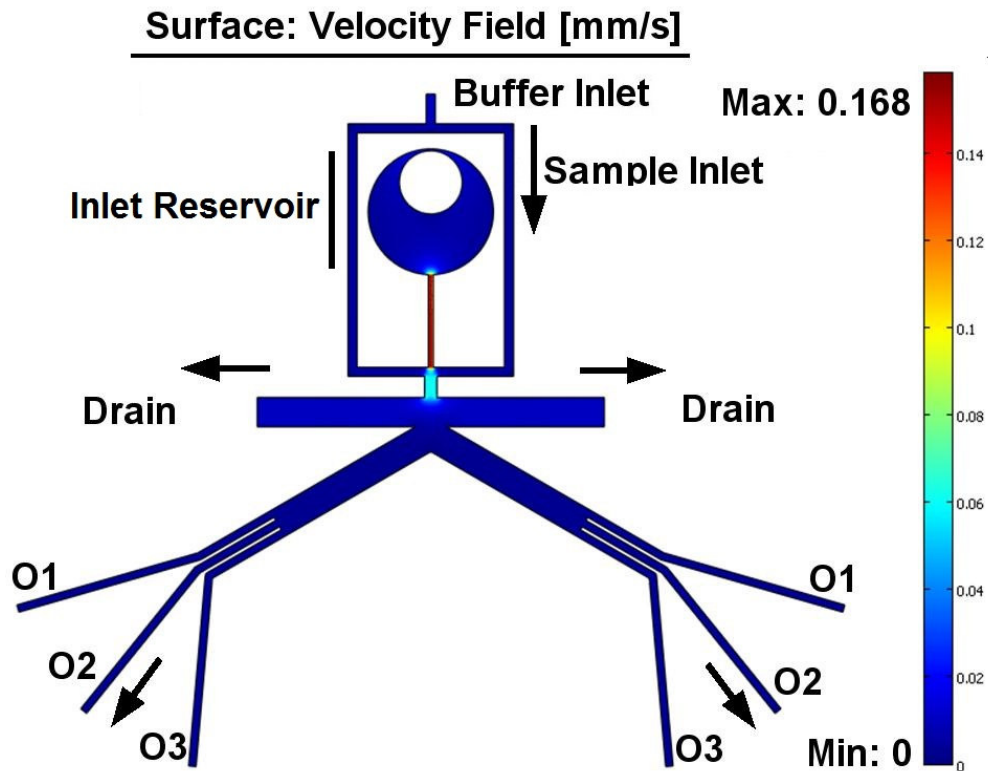
Figure 26. COMSOL model of an entire device.

Arrows above indicate direction of flow. Labels show location of the inlet reservoir, buffer and sample inlets, two drain channels, and collection outlets 1, 2 and 3 (O1, O2, O3). Velocity is highest in the channel exiting the inlet reservoir.
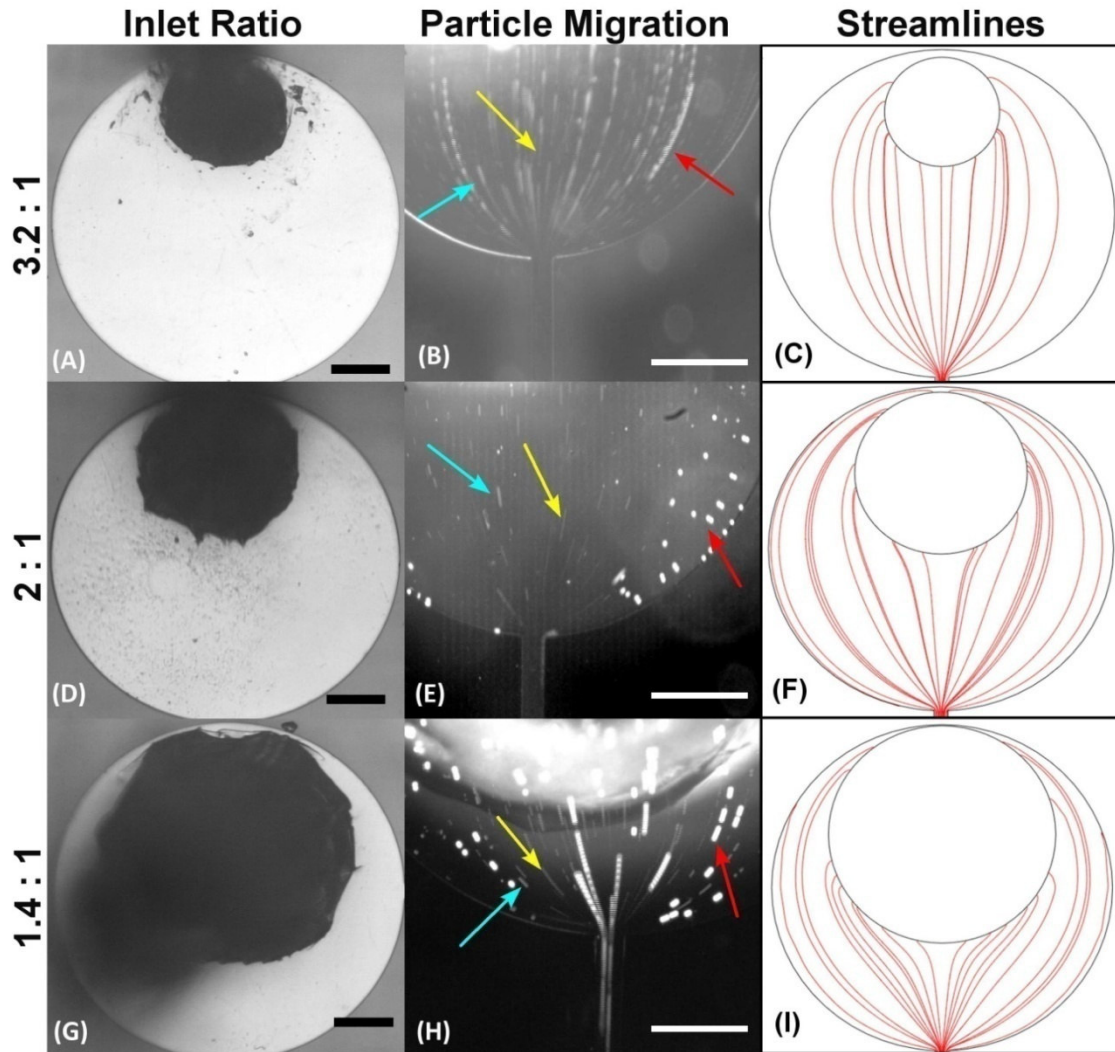
Figure 27. Ratio of inlet reservoir to inlet diameter at 3.2:1, 2:1, and 1.4:1 ratios.

This figure from right to left shows sample inlet connections (black hole) punched into the inlet reservoir (white circle), the resulting migration of a mix of particles, and a COMSOL model demonstrating exiting streamline flow (Scale Bars are 250 µm). Red arrow denotes 10 µm particles, Cyan arrow denotes 5.5 µm particles, and Yellow arrow denotes 3.0 µm particles. Images of particle movements are Image J Z projections of 15 frames at Max Intensity. (A – C) 3.2:1 ratio, (D – F) 2:1 ratio, and (G – I) 1.4:1 ratio placed at the top of the reservoir, the subsequent particle migration trajectory, and COMSOL Model of streamline flow.

3.4 Separation of Particles using Devices with Varying Outlet Widths

As mentioned above, the sample inlet diameter was varied by using different gauge needles to punch the connections into the reservoir (see Figure 27A, D, and G). The initial particle trajectories in the reservoir were the most resolved with inlet ratios of 2:1 as observed both experimentally and through the streamline flows modeled with COMSOL (see Figure 27E and F). Therefore the 2:1 inlet ratio was chosen for initial separation experiments using devices with varying downstream outlet widths: 200 µm, 350 µm, or 500 µm. This set of experiments helped determine the device size that produced the best downstream particle separation. Figure 28 shows the downstream particle distribution through the bifurcation segment and towards the collection outlets. A mix of 10 µm, 5.5 µm, and 3.0 µm particles separated best in devices with 350 µm outlet widths (see Figure 28C).

Table 6 lists the results of separation experiments with different outlet widths. The 350 µm device is listed first for each particle diameter, because the separation efficiency was significant across the three particle diameters. For each device width separately, a One-way ANOVA was performed with collection outlet as the experimental unit and particle diameters as treatment. Only in the 350 µm devices did 10 µm predominately distribute to Outlet 1, 5.5 µm to Outlet 2, and 3.0 µm to Outlet 3 (Fig 28C, Table 6, A superscript, $p < 0.001$). For these reasons only devices with total outlets widths of 350 µm were chosen for subsequent experiments.
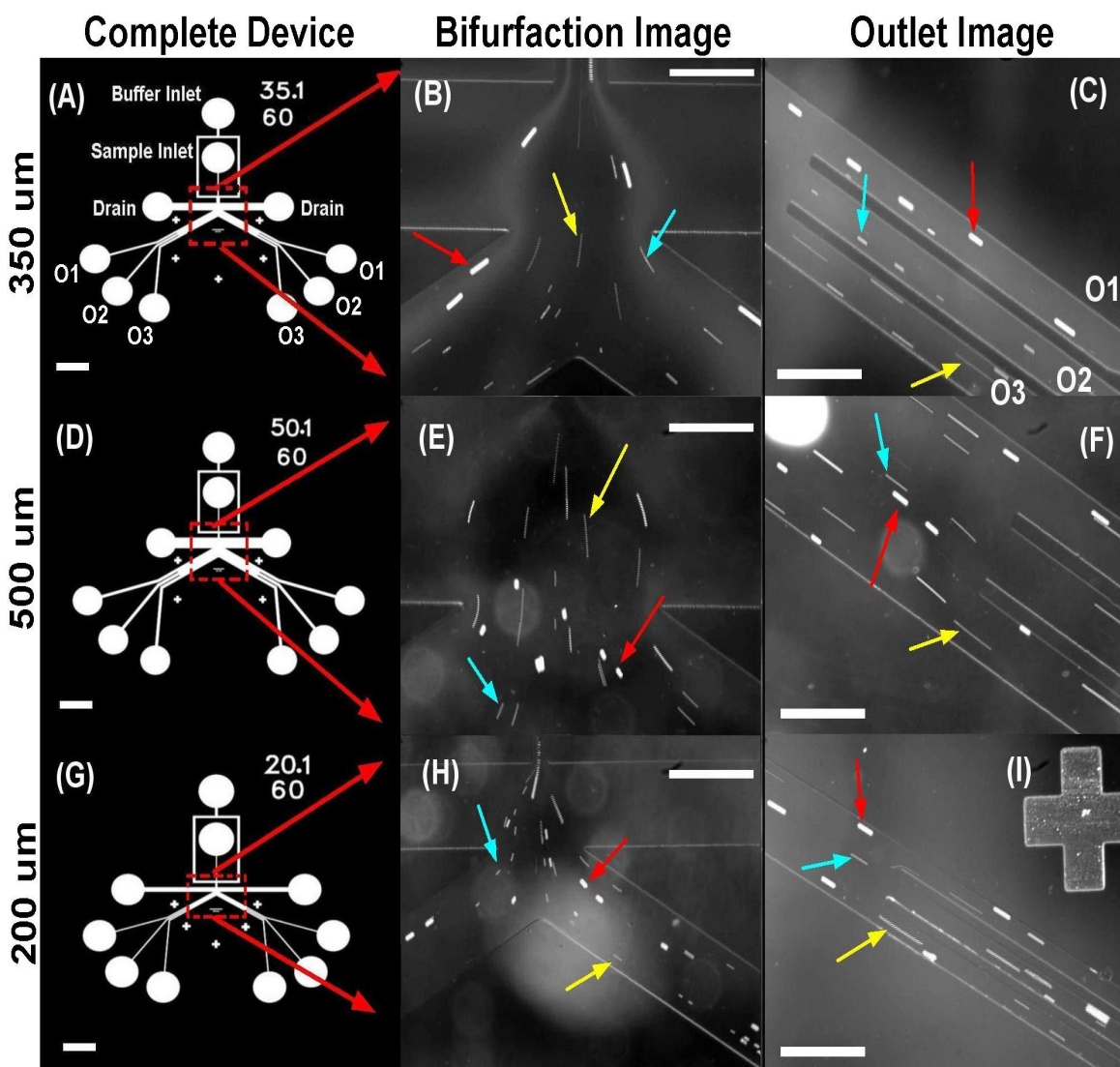
Figure 28. Separation of particles in devices with outlet widths of 200 μm, 350 μm, and 500 μm.

In the figure above the total device is shown for three outlet widths. The red square indicates the portion that is enlarged to show images of the bifurcation segment with particles in motion. The resulting distributions of particles to the collection outlets are also shown. Red arrow denotes 10 μm particles, Cyan arrow denotes 5.5 μm particles, and Yellow arrow denotes 3.0 μm particles. Images of particle movements are Image J Z projections of 15 frames at Max Intensity. (Scale Bars in order from right to left are 1500 μm, 350 μm). (A, B, C) 350 μm width, (D, E, F) 500 μm width, and (G, H, I) 200 μm devices, where 350 μm outlet width had the most significant distribution of particles (see text and Table 5).

Table 6. Separation of Particles from Three Outlet Widths

Particle diameter (µm)	Outlet Width	Distribution Ratio (%)		
		Outlet 1	Outlet 2	Outlet 3
10.0	350 µm	**73.4**[A]	16.9	9.8
	200 µm	56.3	23.2	20.5
	500 µm	45.5	32.7	21.8
5.5	350 µm	9.1	**64.7**[A]	26.2
	200 µm	20.4	50.7	28.9
	500 µm	22.2	43.8	34.0
3.0	350 µm	14.0	33.3	**52.8**[A]
	200 µm	19.0	38.4	42.6
	500 µm	28.8	8.8	62.4

3.5 Separation of Particles using Devices with Varying Inlet Ratios

Having determined that devices with outlets widths of 350 µm (see Table 6) produced the best downstream separation, a set of experiments were conducted to determine if indeed a 2:1 sample inlet ratio in these devices produced significant separation. As shown in Figure 27, the sample inlet diameter was varied by using different gauge needles to punch the connections into the reservoir. Figure 29 shows the downstream distribution of particles to the collection outlets from sample inlet ratios of 2:1, 3.2:1, and 1.4:1.

Figure 29A-C further shows that a 2:1 ratio of inlet reservoir to sample inlet diameter demonstrated the best distribution of particles to all the three collection outlets. This follows from the observed inlet particle trajectories and COMSOL models of streamlines (see Figure 27C). A 3.2:1 inlet ratio was not as efficient in separating

particles, but more so than a 1.4:1 ratio. This is also in agreement with the observed inlet particle trajectories and COMSOL Models.

Table 7 lists the results of separation experiments with different ratios of inlet reservoir diameter relative to the sample inlet diameter. The 2:1 ratio is listed first for each particle diameter, because the separation efficiency was significant across the three particle diameters. For each ratio separately, a One-way ANOVA was performed with collection outlet as the experimental unit and particle diameters as treatment. Only in the 2:1 ratio did 10 µm predominately distribute to Outlet 1, 5.5 µm to Outlet 2, and 3.0 µm to Outlet 3 (Fig 29B, C, Table 7, Asuperscript, $p < 0.001$). In the 3.2:1 and 1.4:1 ratios, the distribution of particles to each outlet was not significantly different. Devices with a 2:1 ratio demonstrated greatest particle distribution for 10 µm particles to Outlet 1, 5.5 µm particles to Outlet 2, and 3.0 µm particles to Outlet 3.

A Two-Sample T-test showed that the 2:1 ratio compared to the 3.2 ratio distributed 10 µm particles to Outlet 1 and 5.5 µm particles to Outlet 2 more significantly (Table 7, B superscript, $p < 0.05$). There was no difference for 3.0 µm particles to Outlet 3 between a 2:1 and a 3.2 inlet ratio. Lastly, there were no significant changes in distribution of 1.1 µm particles to each collection outlet and thus were not included in further experiments (see Table 7). 1.1 µm particles migrating in the inlet reservoir of 2:1 inlet ratio and their subsequent downstream collection outlet distribution are shown in Figure 30. This indicates a lower limit of particle size for separation with this specific device design.
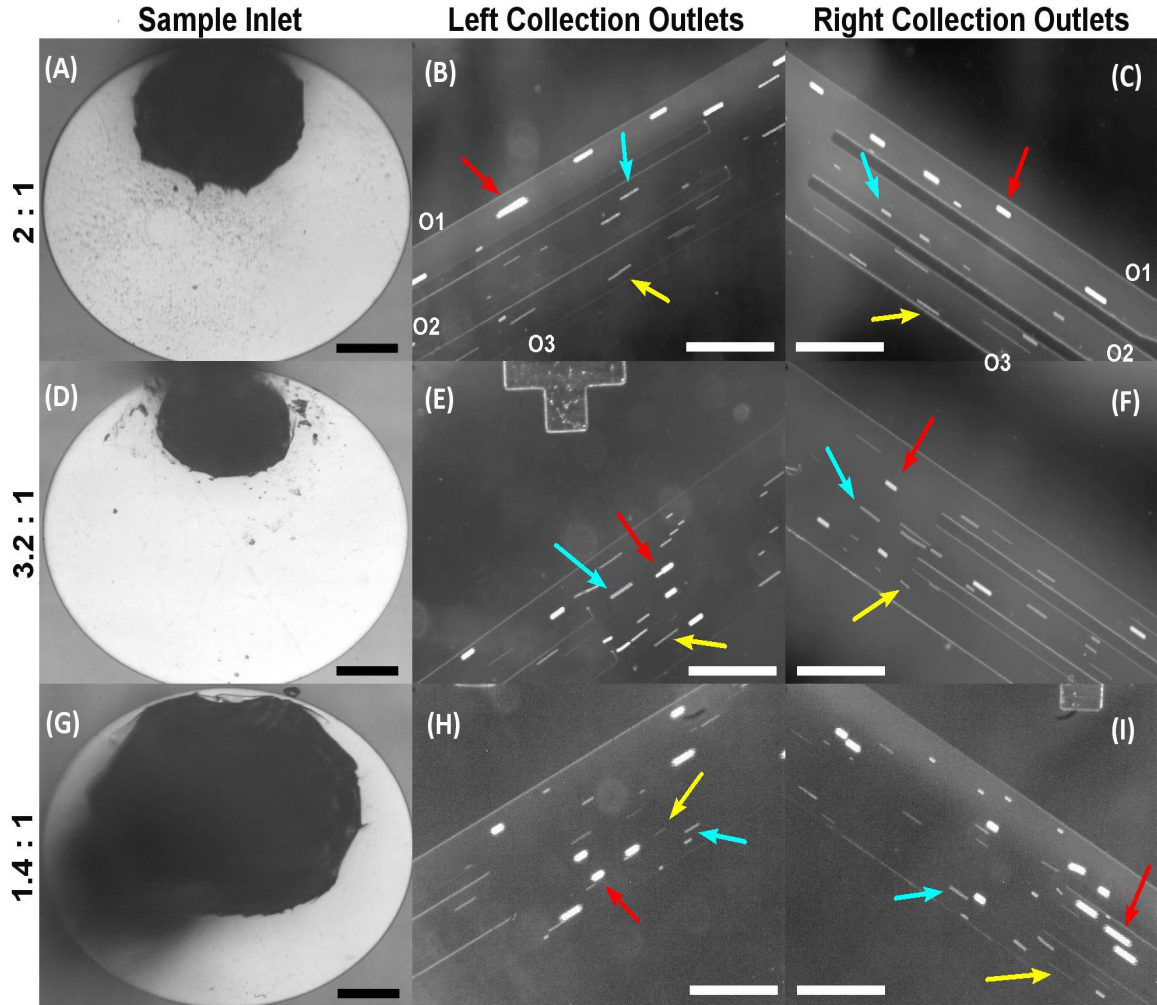
Figure 29. Particle separations in 3.2:1, 2:1, and 1.4:1 ratios using 350 µm devices.

The figure above is a series of images showing the distribution of particles to both the left and right side of the device from 3.2:1, 2:1, and 1.4:1 ratios (Scale Bars are 250 µm). Red arrow denotes 10 µm particles, Cyan arrow denotes 5.5 µm particles, and Yellow arrow denotes 3.0 µm particles. Images of particle movements are Image J Z projections of 15 frames at Max Intensity. Distribution was best for the 2:1 ratio. (A – C) 3.2:1 ratio, (D – F) 2:1 ratio, and (G – I) 1.4:1 ratio placed at the top of the reservoir and their subsequent particle distribution.

Table 7. Separation of Particles from Three Different Inlet Ratios

Particle diameter (µm)	Inlet Ratio	Distribution Ratio (%)		
		Outlet 1	Outlet 2	Outlet 3
10.0	2 : 1	**73.4**[A,B]	18.8	9.8
	3.2 : 1	56.0	28.7	15.3
	1.4 : 1	46.8	26.7	26.3
5.5	2 : 1	9.1	**64.7**[A,B]	26.2
	3.2 : 1	23.5	50.8	25.7
	1.4 : 1	30.6	35.3	34.1
3.0	2 : 1	13.9	33.3	**52.8**[A]
	3.2 : 1	20.2	37.0	42.8
	1.4 : 1	35.2	34.7	30.1
1.0	2 : 1	34.4	33.8	31.8
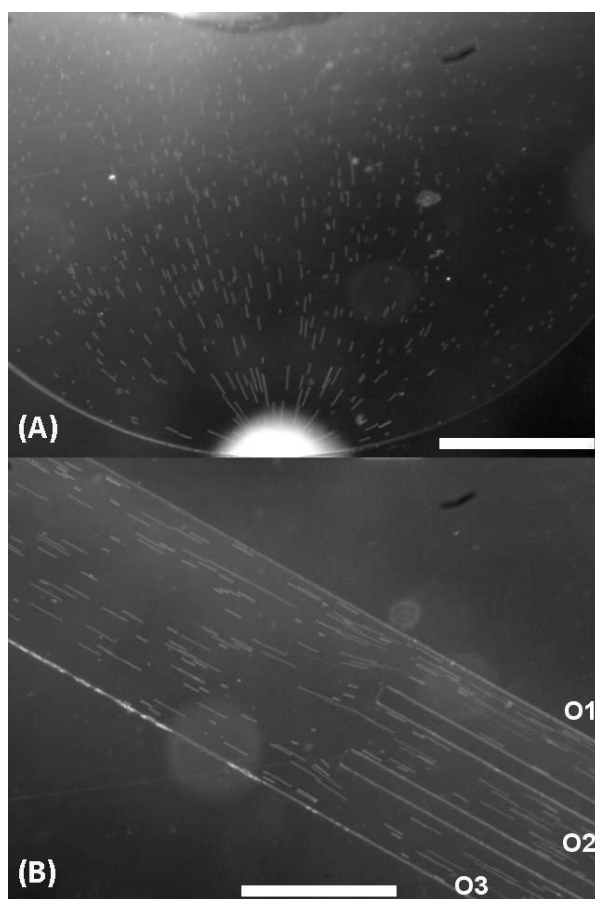
Figure 30. 1.1 µm particle separations.

This figure shows the distributive separation of 1.1 µm particles in a device with 2:1 ratio inlet ratio, 350 µm outlet channel width and collection outlets angle of 60º. Images of particle movements are Image J Z projections of 15 frames at Max Intensity. (A) 1.1 µm particles sample the entire reservoir. (B) This leads to 1.1 µm particles distributing about evenly to each collection outlet (Scale bars are 250 µm).

3.6 Characteristic Sample Inlet (CSI) using Devices with Varying Inlet Ratios

A dimensionless number, the Characteristic Sample Inlet (CSI) was developed to characterize the position and radius of the sample inlet hole relative to the sample inlet diameter, and that effect on downstream distribution of particles. The CSI number is given by:

$$\frac{L}{R-r} \tag{29}$$

where L is the distance from the tip of reservoir to the middle of the inlet, R is the radius of the inlet reservoir, and r is the radius of the sample inlet (see Figure 31 inset).

In equation (29), for a fixed value of L and R, the greater the sample inlet r, the greater the Characteristic Sample Inlet. Figure 31 shows a plot taking only the distribution of 10 µm particles to Outlet 1 from each ratio, 5.5 µm particles to Outlet 2 from each ratio, and 3.0 µm particles in Outlet 3 from each ratio, relative to the Characteristic Inlet of each ratio. With this plot, it is noticeable that at a CSI of 1, corresponding to a 2:1 ratio, distribution of the three particles is best.
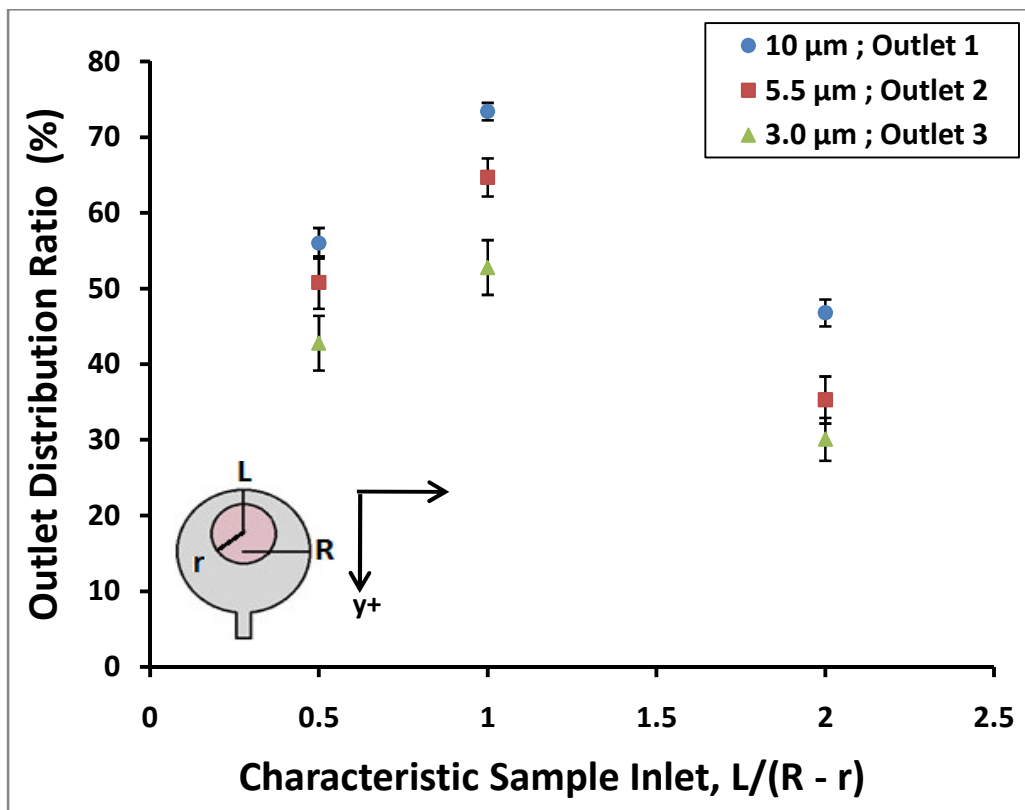
Figure 31. Distribution of particles relative to the Characteristic Sample Inlet.

This graph shows that a CSI value of 1, the distribution ratio for each particle is clearly highest. A CSI value of 0.5 corresponds to a 3.2:1 ratio, a CSI value of 1 to a 2:1 ratio, and a CSI value of 2 to a 1.4:1 ratio.

3.7 COMSOL Models of the Inlet Reservoir with Varying Sample Inlet Diameters

As described in Section 3.3, COMSOL Multiphysics of the inlet reservoir was modeled to analyze how the velocity profiles inside the reservoir affected the initial trajectories of particle migration. Each inlet diameter was placed at the top of the reservoir for all three ratios, 1.4:1, 2:1, and 3.2:1. The same experimental conditions, a sample inlet flow rate of 5 µl/hr and buffer inlet flow rate of 10 µl/hr, were implemented as boundary conditions. Only the steady-state Stokes Flow module was utilized.

Shown in Figure 32 is a horizontal line drawn just below each sample inlet and the velocity profile was plotted across this line. In this region, a particle first experiences the velocity distribution within the reservoir and this subsequently has a direct impact on the downstream separation to the collection outlets. For all three ratios, a velocity minimum is observed in the middle of the reservoir. This parabolic velocity profile is similar to what is observed in a rectangular channel.

These velocity profiles effect on particle migration corroborated with what was observed in Figure 27. As shown in Figure 32A and B, for a 3.2:1 ratio, the narrowness of the two parabolic peaks and largest velocity tended to keep particles closer towards the middle of the inlet reservoir. Also shown in Figure 32C and D, for a 2:1 ratio, the parabolic profile is the most resolved and this allowed particles to spread and establish migration on streamlines further apart in the reservoir. Thus in turn, a 2:1 ratio of inlet reservoir diameter to sample inlet produced the best separation of particles. Lastly, in Figure 32E and F, for a 1.4:1 ratio, the sample inlet was placed too close to the bottom of the inlet reservoir. As the ratio decreased, from 3.2:1, to 2: 1, to 1.4:1, the micron distance between the parabolic peaks increased. Furthermore the difference between the velocity maximum to minimum also increased.
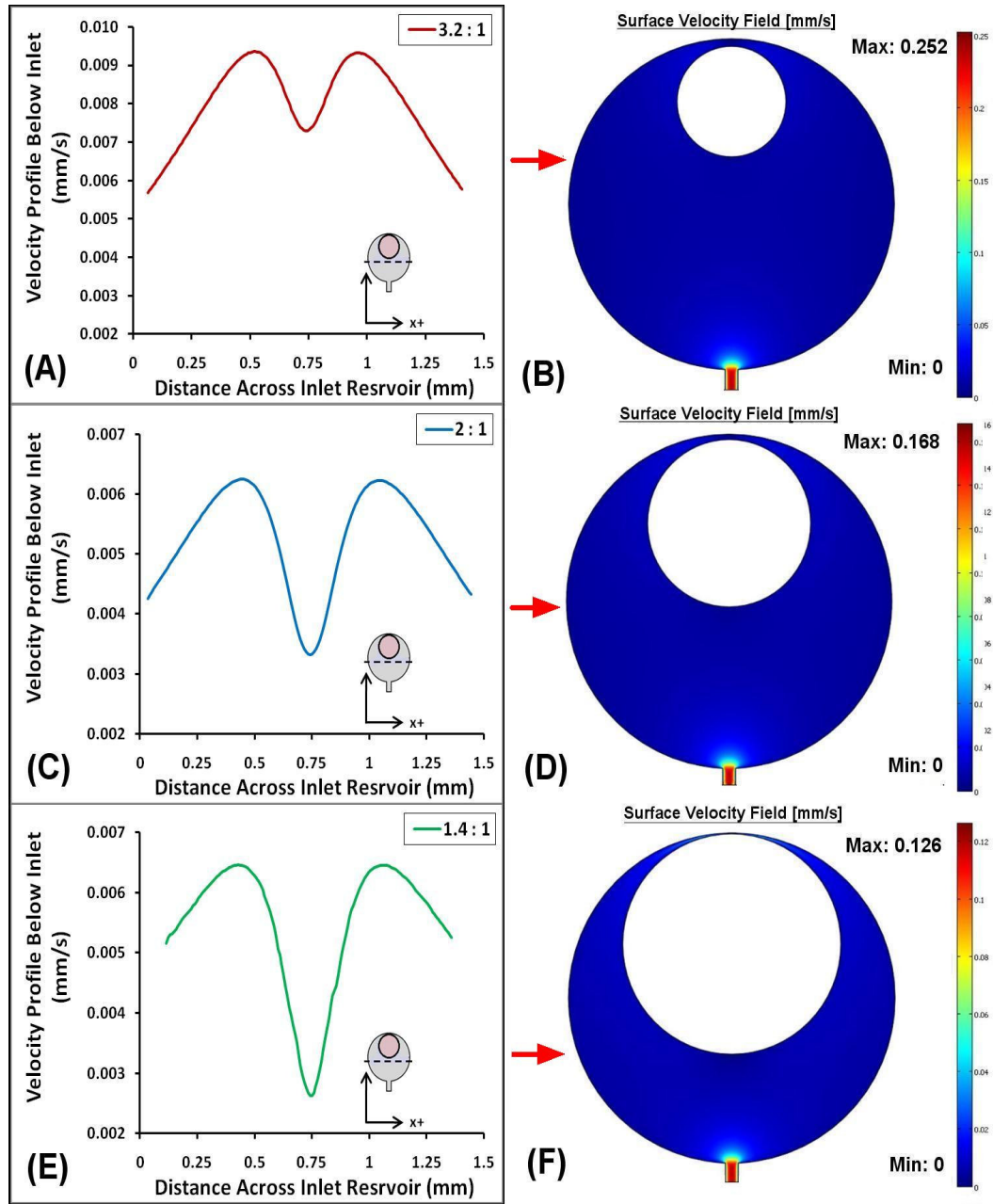
Figure 32. Velocity profile plots across the reservoir of 3.2:1, 2:1, 1.4:1 inlet ratios.

The figure above displays velocity profiles taken with the accompanying COMSOL models for all three inlet ratios, 3.2:1, 2:1, and 1.4:1. The inset schematic in the plot and arrow in the COMSOL image indicates the location in the inlet reservoir where the velocity profile was taken. (A, B) 3.2:1 (C, D) 2:1 and (E, F) 1.4:1 velocity profiles with COMSOL Models.

3.8 Relating Particle Separation to COMSOL derived Velocity Profiles at the Inlet Reservoir

By utilizing the unique velocity profiles modeled and graphed with COMSOL, a way of relating these velocity profiles to the subsequent downstream particle distribution was developed. It was noticed that the parabolic shape of the velocity profiles modeled varied in width and shape depending on the inlet ratio (see Figure 32). These differences in the velocity profiles were characterized by using a dimensionless ratio comparing both sides of the velocity parabola.

Figure 33 is a schematic highlighting the key variables utilized for the dimensionless ratio. The first part of the ratio, m_A is found by taking the difference in maximum reservoir velocity from the velocity at the edge of the reservoir, over the distance between these two velocities:

$$m_A = \frac{V_2 - V_1}{X_2 - X_1} \tag{30}$$

where V_2 is the maximum parabola velocity, V_1 is the velocity at the edge of the reservoir, and X_2 - X_1 is the distance between these two velocities (see Figure 32). The second part of the ratio, m_B is found by taking the difference in maximum reservoir velocity from the minimum velocity at the middle of the reservoir, over the distance between these two velocities:

$$m_B = \frac{V_2 - V_3}{X_3 - X_2} \tag{31}$$

where V_2 is the maximum parabola velocity, V_3 is the minimum center reservoir velocity, and $X_3 - X_2$ is the distance between these two velocities (see Figure 32). The ratio of m_B/m_A for the 3.2:1, 2:1, and 1.4:1 ratios modeled with COMSOL in Figure 32 are provided in Table 8 below.
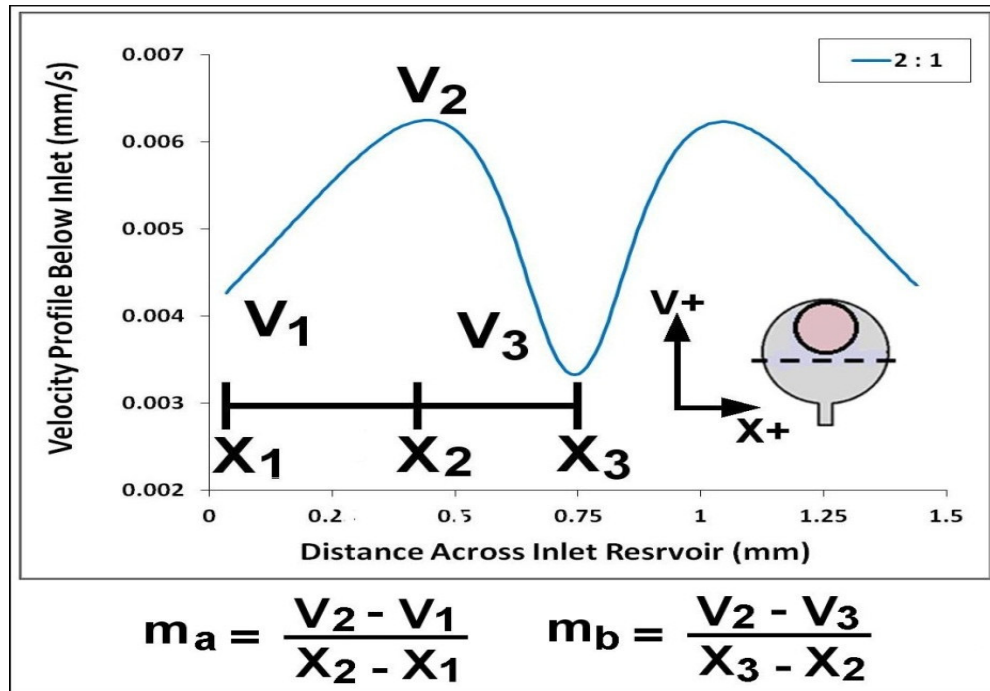
Figure 33. A schematic highlighting the key variables utilized for the dimensionless ratio m_B/m_A. The velocity profile below was taken just below the inlet reservoir modeled with COMSOL.

Table 8. m_b/m_a of Different Inlet Ratios			
Inlet Ratio	**m_b/m_a**	**m_a**	**m_b**
3.2 : 1	1.14	0.008	0.0091
2 : 1	1.91	0.0051	0.0039
1.4 : 1	3.17	0.0097	0.0124

Using values of m_B/m_A provided in Table 8, a plot similar to Figure 31 was constructed. However in this plot, the ratio of m_B/m_A substituted for the Characteristic

Sample Inlet. This plot combines both experimental and computational data and helps demonstrate that at an m_B/m_A close to 2, corresponding to a 2:1 ratio, best downstream distribution of particles occurs. The similarity of Figure 34 to Figure 31 indicates that two separate criteria can be used to demonstrate expected particle distribution, one using a geometric dimensionless number and one from a computationally derived dimensionless ratio. The computational model verifies experimentally why a 2:1 ratio placed at the top of the reservoir produced the best separation results.
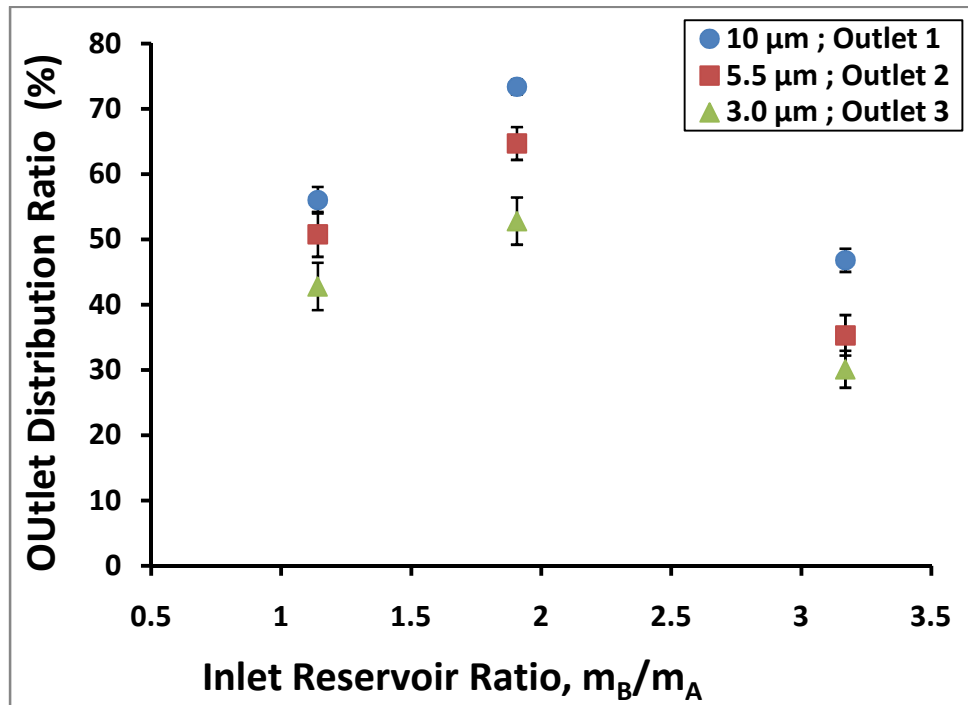
Figure 34. Distribution of particles relative to the relative ratio m_B/m_A.

The distributions of particles in this plot are identical to Figure 31; however these values were related to the ratio m_B/m_A found using COMSOL Models. The same pattern exists as Figure 31, where a 2:1 inlet ratio, corresponding to an m_B/m_A of 1.91 had the most significant distribution of particles. This plot therefore relates experimental data and computational data.

3.9 The Inlet Reservoir with Varying Sample Inlet Positions with a 2:1 Ratio

Having established that the 2:1 ratio produced the best downstream separation (see Table 7), a set of experiments were carried out to determine if the position of the sample inlet was important for significant downstream separation of particles. To determine this, a set of experiments were conducted by varying the sample inlet relative to the inlet reservoir at three different positions: top, middle, and bottom.

Figure 35 shows that as the position of the inlet was placed closer to the bottom of the reservoir, the particle migration trajectory becomes more focused towards the channel exiting the reservoir. This migration path is shown with COMSOL models demonstrating the streamline flow pattern (see Figure 35C, F, and I). An inlet position at the top, compared to the middle and bottom of the reservoir, allowed particles to migrate and spread along different streamlines without bunching.
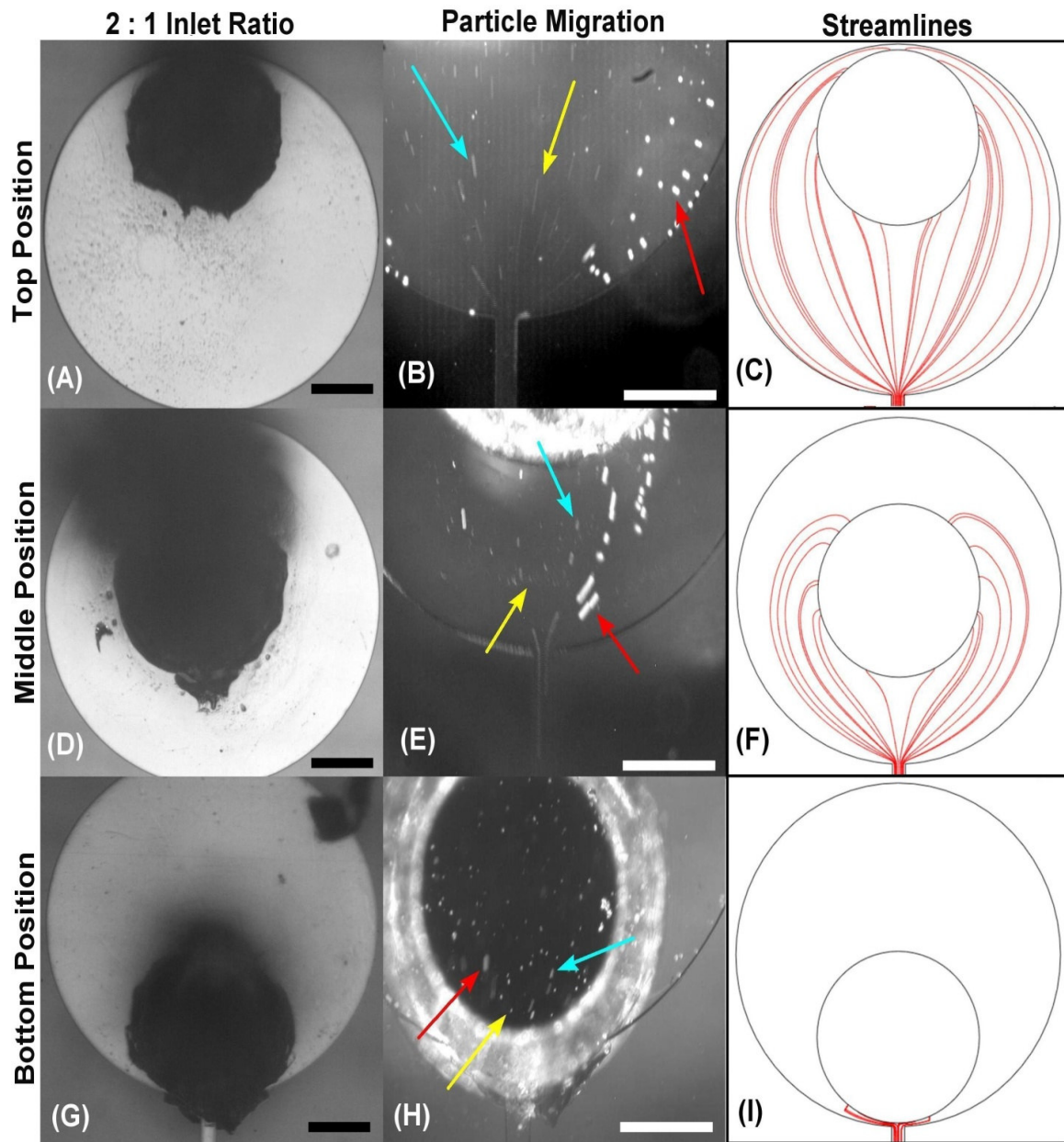
Figure 35. Top, Middle, and Bottom Inlet positions in a 2 : 1 ratio.

A series of images showing a sample inlet connection diameter (black hole) punched into the inlet reservoir (white circle) at different positions, the resulting migration of a mix of particles, and a COMSOL model demonstrating exiting streamline flow (Scale Bars are 250 µm). Red arrow denotes 10 µm particles, Cyan arrow denotes 5.5 µm particles, and Yellow arrow denotes 3.0 µm particles. Images of particle movements are Image J Z projections of 15 frames at Max Intensity. (A – C) Top position of the 2:1 ratio, (D – F) middle position of the 2:1 ratio, and (G – I) bottom position of the 2:1 ratio relative to the reservoir, the subsequent particle migration trajectory, and Comsol Model of streamline flow.

69

3.10 Separation of Particles from a 2:1 Inlet Ratio at the Top, Middle, and Bottom Inlet Reservoir Positions

Figure 36 shows images of the downstream distribution of 10 µm, 5.5 µm particles, and 3.0 µm particles to the collection outlets as a result of varying sample inlet positions from Figure 35. As the inlet was placed progressively closer to the bottom of the reservoir, the distribution ratio decreased for all particles (see Figure 36). At the top position, the streamlines to which the particles flow have sufficient space to initially separate and sample the entire inlet reservoir before exiting. By placing the inlet position towards the bottom of the inlet reservoir and therefore closer to the channel exiting the reservoir, the streamlines particles flow are more condensed and do not sample the entire reservoir (see Figure 35C, F, and I). Instead particles exit the reservoir closer together and do not distribute to separate outlets well.

The distribution ratio of particles to the collection outlets from Figure 36 is shown in Table 9. A Two Sample t-test showed that the top inlet position compared to the middle position distributed 10 µm particles to Outlet 1 and 5.5 µm particles to Outlet 2 more significantly (Table 9, A superscript, $p < 0.05$). Lastly there was no difference for 3.0 µm particles to Outlet 3 between any of the sample inlet positions.
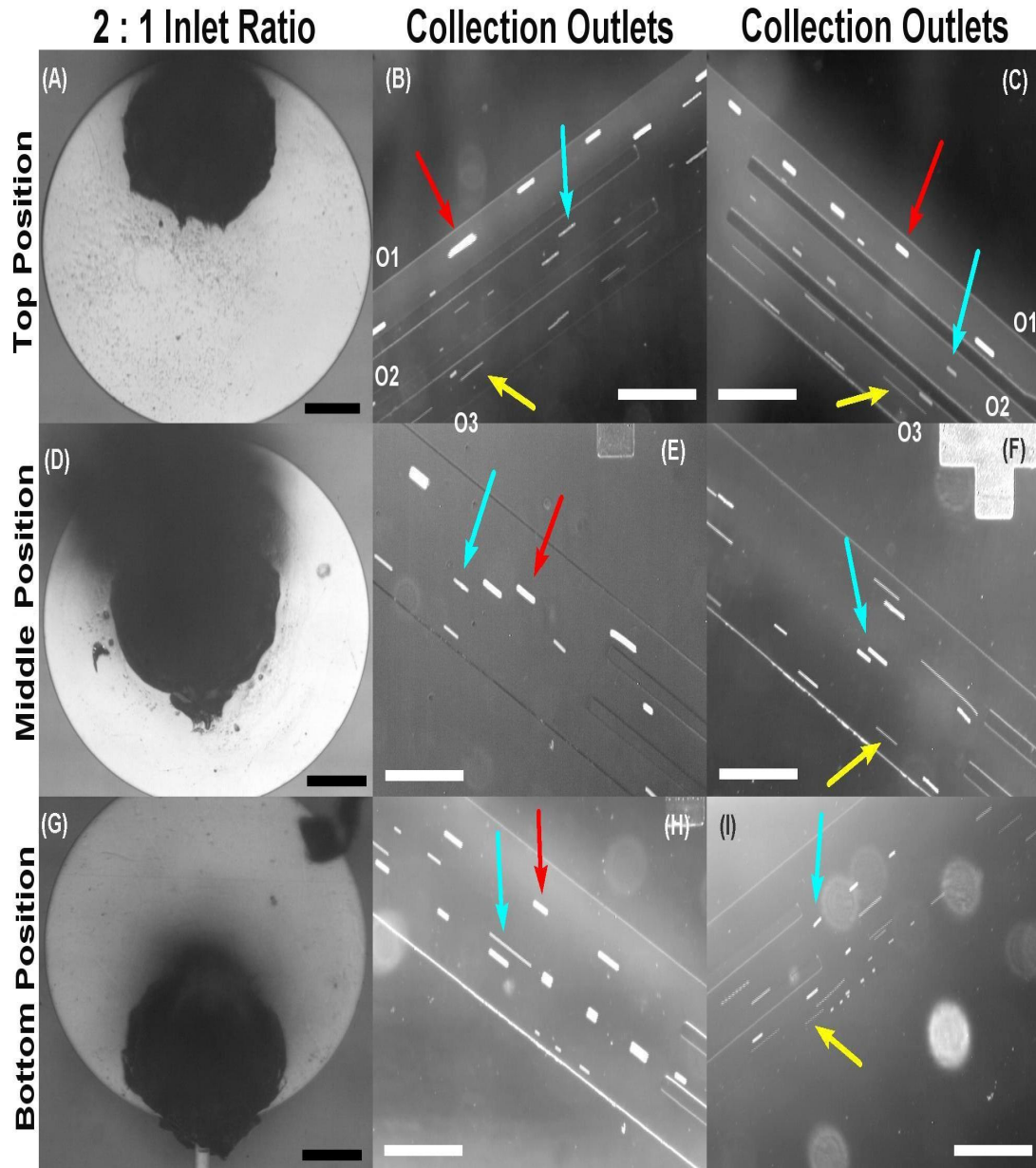
Figure 36. Particle separations of the 2:1 inlet ratio at the top, middle, and bottom positions.

The figure above is a series of images showing particle distribution of the 2:1 ratio at top middle and bottom ratios. (Scale Bars are 250 µm). Distribution was best for the 2:1 ratio. Red arrow denotes 10 µm particles, Cyan arrow denotes 5.5 µm particles, and Yellow arrow denotes 3.0 µm particles. Images of particle movements are Image J Z projections of 15 frames at Max Intensity. (A – C) Top position and particle distribution on the left and right side, (D – F) Middle position and (G – I) Bottom position with two separation images, one with only 10 µm and 5.5 µm particles and another with only 5.5 µm and 3.0 µm particles.

Table 9. Separation of Particles from Three Different 2:1 Ratio Positions

Particle diameter (µm)	Inlet Positions	Distribution Ratio (%)		
		Outlet 1	Outlet 2	Outlet 3
10.0	Top	**73.4**[A]	16.9	9.8
	Middle	52.4	39.7	7.9
	Bottom	5.2	42.8	52.0
5.5	Top	9.1	**64.7**[A]	26.2
	Middle	14.6	45.3	40.2
	Bottom	8.9	37.3	53.8
3.0	Top	14.0	33.3	52.8
	Middle	16.9	41.6	41.6
	Bottom	18.9	36.1	45.0

3.11 Relating CSI to Particle Distribution with Varying Sample Inlet Position

The three inlet positions, top, middle and bottom, were defined with the Characteristic Sample Inlet (CSI) dimensionless number using equation (29). This equation was applied using a fixed inlet reservoir radius, R, and sample inlet radius, r. Only the sample inlet position, L, varied. As this length L increased, the CSI increased from 1 to 3 corresponding to an inlet position from the top to the bottom. Figure 37 shows a plot taking only the distribution of 10 µm particles to Outlet 1 from each ratio, 5.5 µm particles to Outlet 2 from each ratio, and 3.0 µm particles in Outlet 3 from each ratio, relative to the Characteristic Inlet of each inlet position. With this plot, it is seen that a CSI of 1, corresponding to a top inlet position, distributed particles of three different diameters better than the middle or bottom positions.
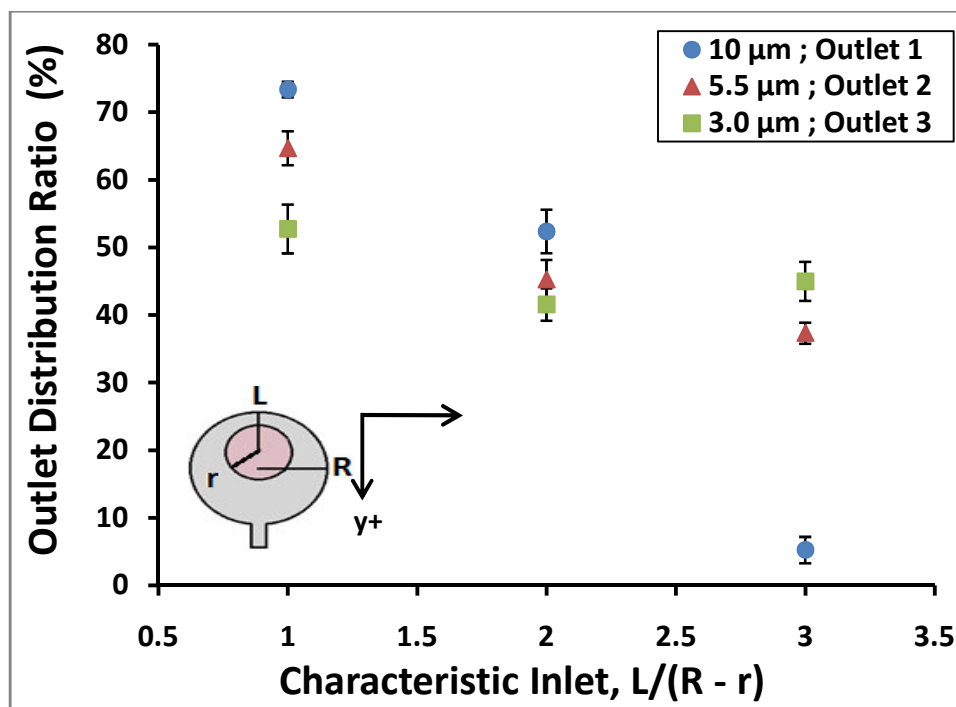
Figure 37. Characteristic Sample Inlet Plot for the 2:1 ratio at top, middle, and bottom inlet positions.

This graph shows that as the CSI value increases, the downstream distribution of particles decreases. A CSI value of 1 corresponds to the top inlet position, a CSI value of 2 to a middle position, and a CSI value of 3 to a bottom position.

3.12 COMSOL Models of the Inlet Reservoir with Varying Sample Inlet Position

Using COMSOL Multiphysics the inlet reservoir was modeled to analyze how the velocity profiles inside the reservoir affected the initial trajectories of particle migration. A 2:1 inlet ratio was placed at three different positions relative to the inlet reservoir, top, middle, and bottom. The same experimental conditions, a sample inlet flow rate of 5 µl/hr and buffer inlet flow rate of 10 µl/hr, were implemented as boundary conditions. Only the steady-state Stokes Flow module was utilized.

As shown in Figure 38, a horizontal line was drawn just below each sample inlet and the velocity profile was plotted across this line. In this region, a particle first

experiences the velocity distribution within the reservoir and this subsequently has a direct impact on the downstream separation to the collection outlets. For all three ratios, a velocity minimum is observed in the middle of the reservoir. This parabolic velocity profile is similar to what is observed in a rectangular channel.

For all three positions, a velocity minimum is observed in the middle of the reservoir. As the inlet position was placed closer to the bottom of the reservoir the velocity profile narrowed and skewed inwards (see Figure 38B, D, and F). Furthermore the velocity maximum also increased. This experimentally pushed particles towards the middle of the reservoir preventing particles from spreading and establishing migration on streamlines further apart in the reservoir, and therefore poor downstream particle distribution to separate collection outlets.
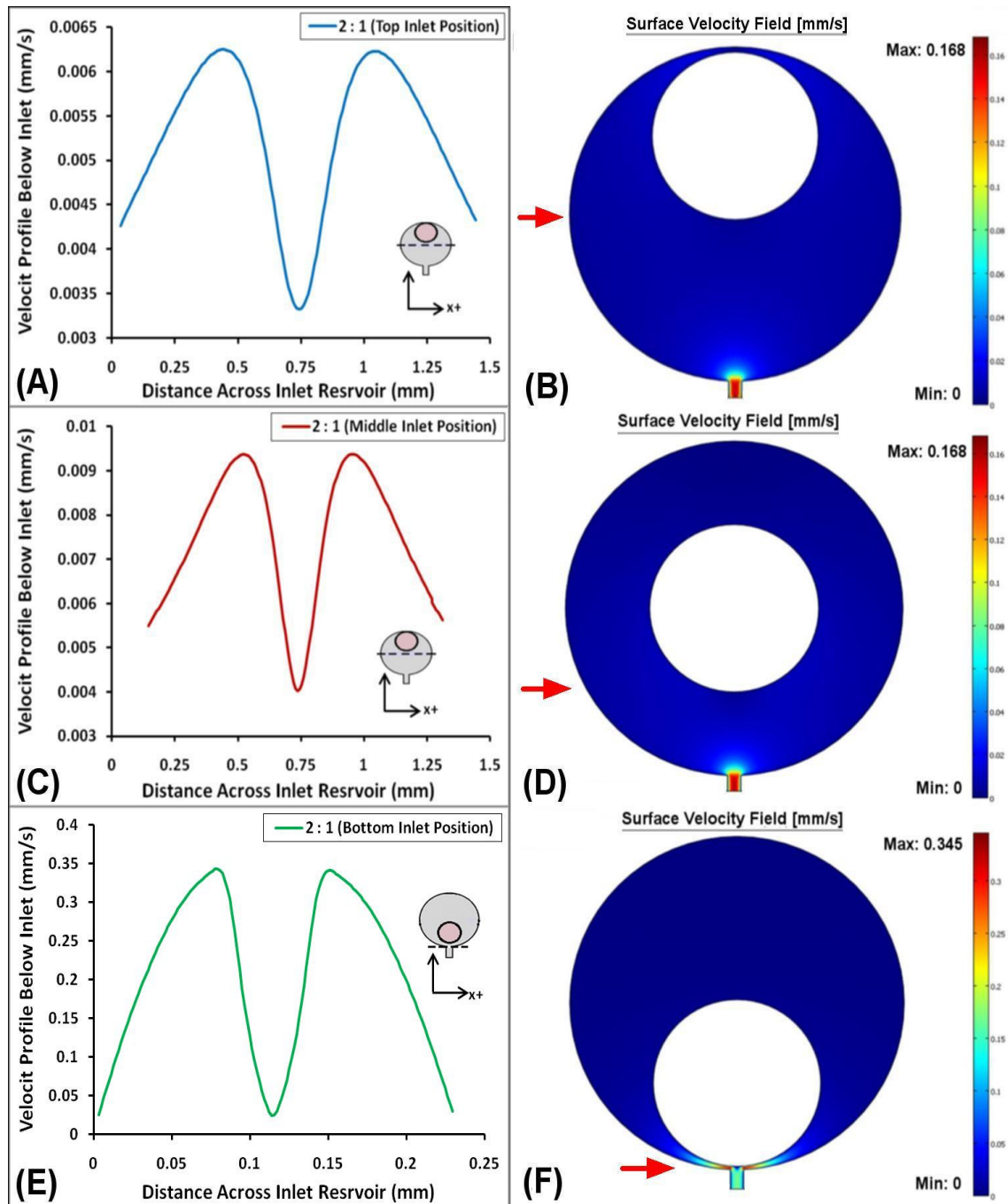
Figure 38. Velocity profile plots across the reservoir 2:1 ratios at top, middle, and bottom positions.

The figure above displays velocity profiles taken with the accompanying COMSOL models for all three inlet positions. The inset schematic in the plot and arrow in the COMSOL image indicates the location in the inlet reservoir where the velocity profile was taken. (A, B) Top (C, D) Middle, and (E, F) Bottom velocity profiles with COMSOL Models from a 2:1 inlet ratio.

3.13 Relating Particle Separation to the Velocity Profiles of Varying Sample Inlet Position

By utilizing the unique velocity profiles modeled and graphed with COMSOL, a way of relating these velocity profiles to the subsequent downstream particle distribution was developed. It was noticed that the parabolic shape of the velocity profiles modeled varied in width and shape depending on the position of the sample inlet (see Figure 38). These differences in the velocity profiles were characterized by using a dimensionless ratio, m_B/m_A, comparing both sides of the velocity parabola as developed in Section 3.8

Figure 39 is again a schematic highlighting the key variables utilized for the dimensionless ratio, $\mathbf{m_B/m_A}$. The ratio of m_B/m_A for top, middle and bottom sample inlet positions modeled with COMSOL in Figure 38 are provided in Table 10 below.
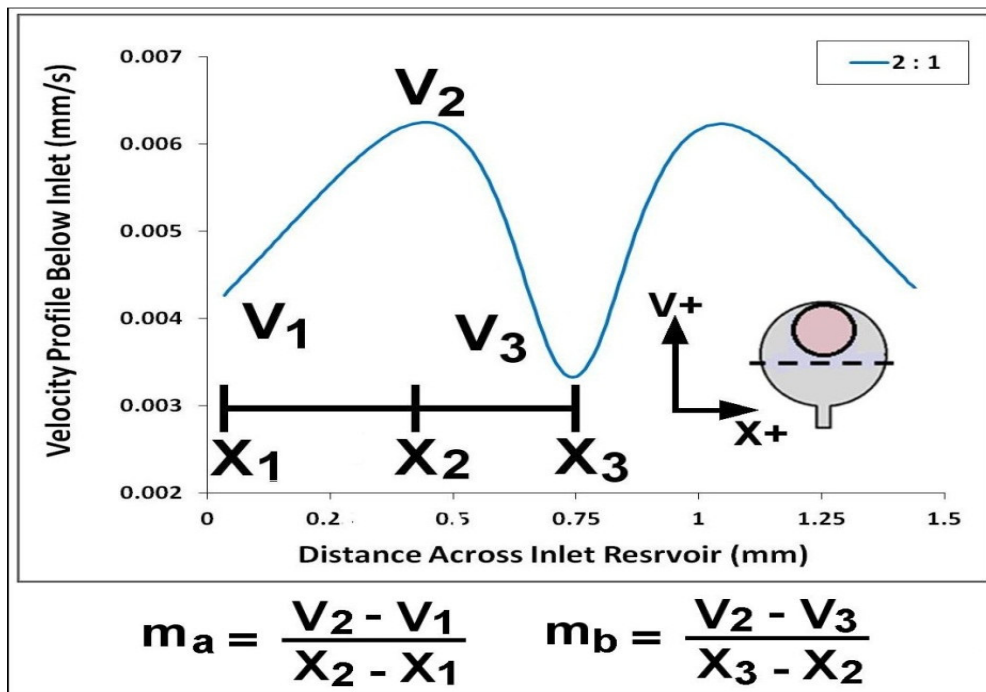
Figure 39. A schematic highlighting the key variables utilized for the dimensionless ratio m_B/m_A. The velocity profile below was taken just below the inlet reservoir modeled with COMSOL.

Using the ratios provided in Table 10, a plot similar to Figure 37 was constructed (see Figure 40). However in Figure 40, the ratio **m_B/m_A** was substituted for the Characteristic Sample Inlet. In this plot the same downstream distribution of particles plotted in Figure 37 were used, but instead related to the **m_B/m_A** of each sample inlet position. This plot combines both experimental and computational data and helps demonstrate that at an **m_B/m_A** close to 2, corresponding to a top inlet position, best distribution of particles occurs.

The similarity of Figure 40 to Figure 37 indicates that two separate criteria can be used to demonstrate expected particle distribution, one using a geometric dimensionless number and one from a computationally derived dimensionless ratio. The computational model verifies experimentally why a 2:1 ratio placed at the top of the reservoir produced the best separation results. Therefore two parameters that can be met in this device design to generate significant particle separation, a CSI value of 1 and a relative velocity ratio m_B/m_A close to 1.91.
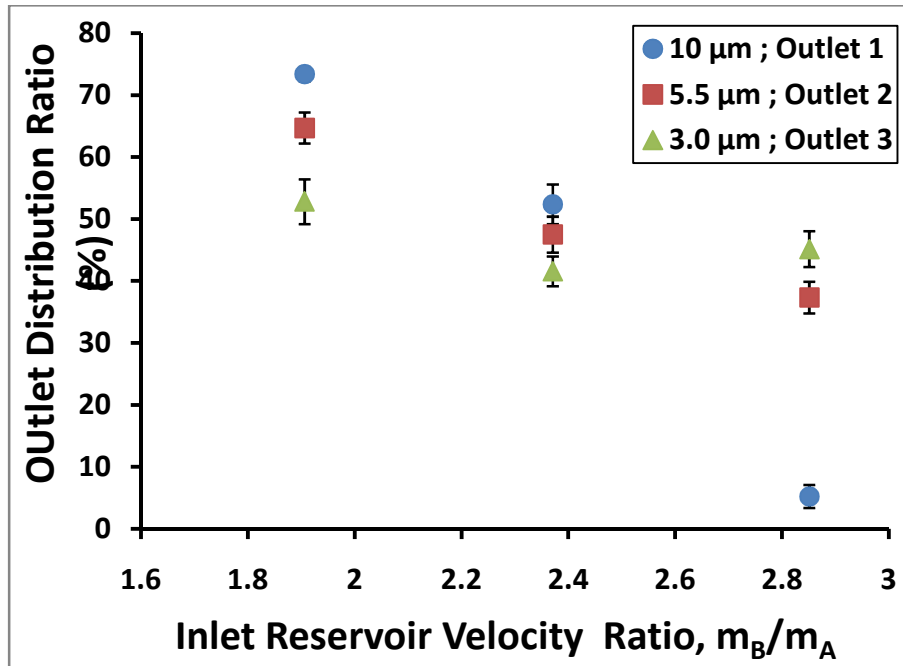
Figure 40. Distribution of particles relative to ratio m_B/m_A from top, middle, and bottom inlet positions of a 2:1 ratio.

The distributions of particles in this plot above are identical to Figure 37; however these values were related to ratio m_B/m_A found using COMSOL Models. The same pattern exists from Figure 37, where a top position, corresponding to an m_B/m_A of 1.91 had the most significant distribution of particles. This plot therefore relates experimental data and computational data.

Table 9. m_b/m_a of Different 2:1 Inlet Positions			
Inlet Ratio	m_b/m_a	m_a	m_b
2 : 1 (Top)	1.91	0.0047	0.0097
2 : 1 (Middle)	2.37	0.0103	0.0245
2 : 1 (Bottom)	2.85	3.6088	10.289

Discussion/Conclusion

In this project an equivalent circuit model was successfully used to design a microfluidic chip. Utilizing the analogous circuit components of voltage drop, current, and electrical resistance to pressure drop, flow rate, and hydraulic resistance respectively, an entire microfluidic chip was created with control over the microscale fluid mechanics through each outlet channel. The relative proportion of outlet flow rates through both the drain and collection outlets were not changed regardless of the set inlet flow rate due to the fixed hydraulic resistance of all the outlet channels. This was accomplished using the equivalent circuit model. Roughly 80% of the initial flow rate was carried through both drain channels, and the remaining 20% flow rate through six collection outlet channels. This project demonstrated the usefulness of first taking advantage of the equivalent calculations between an electrical circuit and integrated microfluidic circuit when designing a chip for any range of experimental applications.

Fabrication of the microfluidic chips employed the methodology and technique of soft lithography. The chip was designed with simplicity in mind as a single layer device whose operation would be performed under continuous flow. With that in mind, any technique that creates feature sizes of 20 µm tall channels with a minimum width of 75 µm for the collection outlets could be used. Soft lithography using SU-8 molds has the advantage that channels are made smooth with the desired rectangular cross section. However the PDMS casting mold does not hold up over time to repeat use and its gas permeability make it difficult to force air bubbles out of the microchannels during a continuous flow experiment. On the other hand for fast and quick proof of concept type

experiments, PDMS chips can fill that criterion. It's relatively cheap cost, fast cure time, and transparency is all important aspects in microfluidic research. Outside of a research context and out to the real world field, a material more durable than PDMS must be utilized, especially if the end goal is developing a field based diagnostic µTAS.

In separation experiments with a mixture of particle diameters, to ensure that each particle diameter was sampled in even proportion, stock concentrations of particles were diluted down to a working concentration of 2.1 x 10^5 particles/µl (see Table 5). Flow rates used were relatively slow at 5 and 10 µl/hr for both the sample and buffer inlets respectively. Since video recordings taken at 7 frames/second were the main method for data collection, the relatively slow flow rates guaranteed accurate counting was achieved during analysis. Even at these flow rates, the total number of particles entering the collection outlets was large, ranging from 3900 particles/hr for 10 µm particles to 4200 particles/hr for 1.1 µm particles (see Figure 25). The separation experiments with mixtures of particles were therefore carried out with a consistent distribution of particles among the different diameters and at flow rates easily detectable using video recordings.

Initial experiments found that a 2:1 geometric ratio of inlet reservoir diameter to sample inlet diameter distributed particles with even spread throughout the reservoir. The other geometric ratios either distributed particles too narrowly as in the case of 3.2:1 ratio or in the case of 1.4:1 ratio the inlet diameter was too large to allow particles to broadly distribute within the reservoir (see Figure 27). Inlet reservoir COMSOL models of the different sample inlet ratios showed that the flow streamlines within the reservoir corroborated with the experimental observations of particle migration. COMSOL models in the future can provide an initial quick observation of the expected particle migration

patterns for a given sample inlet and reservoir diameters. Larger particles entering the reservoir tended to migrate out towards the periphery of the reservoir while smaller particles stayed closer to the middle. In turn this had an effect on the downstream distribution of the particles. Larger particles from the periphery was shown to significantly distribute to the outside Collection Outlets 1, while smaller particles from the middle of the reservoir distributed to the inside Collection Outlets 3 (see Figure 29). Particles of intermediate size distributed to the middle Collection Outlets 2.

COMSOL models from Figure 32 of the different inlet ratios were used to derive values for the Drag force, Reynolds particle number, and Peclet number for each particle diameter tested. These values are shown below in Table 10 and were derived in Section 1.6 fitting with the theoretical range discussed. It can be seen for all particles, the $Re_p \ll 1$, indicating that as particles entered the reservoir they flowed and accelerated along trajectories determined by the fluid velocity profile within the reservoir. Each inlet ratio in turn created different velocity profiles that had different effects on the particle migrations, demonstrated by the streamline flows in Figure 27. Bigger particles were slowed down upon entering the reservoir due to viscous drag, allowing them spread to the periphery of the reservoir and creating the initial separation between small and large particles. It is the distinct velocity profiles due to the different inlet ratios that determined how effective initial separation in the reservoir would be. Lastly, since the $Pe \gg 1$ for all particles, it confirmed that the inertial effect of fluid flow contributed a dominant force on particle behavior.

Table 10. Characteristic Microfluidic Particle Values

Particle diameter (µm)	Inlet Ratio	F_D (N)	Re_p	Pe
10	3.2 : 1	9.2E-13	3.9E-05	2594.2
	2 : 1	6.1E-13	2.6E-05	1705.4
	1.4 : 1	5.8E-13	2.6E-05	1579.1
5.5	3.2 : 1	5.0E-13	1.1E-05	1426.8
	2 : 1	3.3E-13	8.0E-06	938.0
	1.4 : 1	3.2E-13	7.8E-06	868.5
3.0	3.2 : 1	2.7E-13	3.5E-06	778.25
	2 : 1	1.8E-13	2.4E-06	511.6
	1.4 : 1	1.7E-13	2.3E-06	473.7
1.1	3.2 : 1	9.8E-14	4.7E-07	259.4
	2 : 1	6.5E-14	3.2E-07	162.8
	1.4 : 1	6.2E-14	3.2E-07	157.9

Three separate experiments, conducted in a sequential manner determined that devices with total outlet widths of 350 µm microns, a 2:1 inlet ratio, and placed at the top of the reservoir produced the most significant downstream separation of three particles. The first experiment focused on channel outlet widths, 200, 350, and 500 µm, in order to find the chip size that would generate significant separation. The results showed that only devices with outlet widths of 350 µm did a One-way ANOVA demonstrate significant separation. This was most likely due to the fact that the collection outlet widths were either too large in the case of the 500 µm outlet widths, or too small in the case of the 200 µm outlet widths (see Figure 28). It should be noted that only three collection outlet widths were designed and fabricated in order to optimize one particle diameter to one collection outlet. If more than three collection outlets were fabricated, the 500 µm device may have performed better. Furthermore if more than three particles are to be separated at one time, more than three collection outlets would need to be fabricated.

The second set of separation experiments focused on chips with different inlet ratios, 2:1, 1.4:1 and 3.2:1, and placed at the top of the reservoir. The results showed that indeed only devices with a 2:1 inlet ratio achieved significant downstream separation (see Table 7). 1.1 µm particles distributed in relative proportion to all three collection outlets. This indicates a lower limit for particle diameters when trying to achieve separation.

The final set of experiments determined the impact of sample inlet position on downstream particle distribution by varying the 2:1 ratio to three positions. While the first two sets of experiments showed that devices with a 2:1 ratio and 350 µm outlet widths gave the best separation results, the sample position had remained fixed at the top of the reservoir. Placing the 2:1 ratio at the top of the reservoir compared to the middle or bottom, significantly improved downstream particle distribution (see Figure 36 and Table 9). Only at the top position were streamlines evenly distributed throughout the reservoir allowing for particles entering the space necessary to initially separate, before exiting downstream to the collection outlets. At the middle or bottom, particle path migration was too condensed and narrowed, resulting in poor initial separation within the reservoir.

The dimensionless number, Characteristic Sample Inlet (CSI), equation 29, was developed to relate the radii of both sample inlet (r) and reservoir (R), with respect to position (L) of the sample inlet along the y-axis of symmetry (see Figures 31 and 37). This dimensionless number based on geometric parameters could then be plotted with respect to downstream particle distributions. In Figure 31, the r term in Equation 29 was adjusted for different sample inlet radii, while sample inlet position was kept fixed at the top of the reservoir. A resulting CSI value of 1 corresponding to a 2:1 ratio had the

highest percentage distribution among three particle diameters. This was in accordance with the statistical significance found for the 2:1 ratio with One-way ANOVA (see Table 7). Additionally, Figure 37 showed that by varying the sample inlet position L, but fixing the sample inlet diameter within the reservoir, a CSI value of 1 also had highest percentage distribution among three particle diameters. Again this was in accordance with statistical significance (see Table 9). Taken together, both plots make the conclusion that by placing the sample inlet at the top of the reservoir at an inlet ratio of 2:1, significant downstream particle separation results.

COMSOL models of the sample inlet and reservoir revealed that the velocity profile across the reservoir differed based on inlet ratio and inlet position. The different width, amplitude, and parabolic skew of each velocity profile within the inlet reservoir, in turn had significant impact on downstream particle distribution. To utilize the uniqueness of each velocity profile, a way to compare them was developed using a dimensionless ratio, m_B/m_A, diagrammed in Section 3.8 (see Figure 33). With this dimensionless ratio, the velocity maximum and minimums as well as the left and right skew of each velocity profile could be accounted for and plotted with respect to downstream particle distribution. Figure 34 demonstrated this through a plot that combined both computational results with COMSOL modeling and actual experimental results. Again the 2:1 ratio (m_B/m_A value of 1.91) compared to 3.2:1 and 1.4:1 ratio had significant downstream separation for three particle diameters. It is particularly easy to see that for each particle diameter in Figure 34, the downstream percentage distribution was highest only in the 2:1 ratio. Figure 40 utilized COMSOL models of the 2:1 inlet ratio placed at

different positions to show again that an m_B/m_A value of 1.91 (top position), helped produce best downstream particle distribution.

Interestingly, Figures 34 and 31 have very similar patterns. However for both figures, the downstream particle distribution was plotted relative to two different dimensionless parameters. In the case of Figure 34, downstream distribution was plotted relative to COMSOL modeling of the inlet reservoir, utilizing just computational derived velocity profiles. In contrast with Figure 31, particle distribution was plotted relative to the CSI, utilizing only simple experimentally determined geometric relations of the reservoir and inlet diameter. Together both plots make the same argument, that the 2:1 ratio had the most significant separation among three particle diameters. Furthermore, Figures 40 and 37 also had similar plot trends, demonstrating again the ability of each plot to link downstream particle distribution to characteristics of the inlet reservoir either using COMSOL models or geometric ratios. In both these plots, the sample inlet was adjusted to three positions and significant separation occurred only when the 2:1 sample inlet ratio was placed at the top the reservoir.

In summary this project developed a passive separation microfluidic device using an equivalent circuit as a model. The chip had a simple single layer design utilizing symmetry to precisely control fluid flow through two drain channels and six total collection outlets. Three particles, diameters 10, 5.5, and 3.0 µm, were significantly separated to three different outlet channels on both sides of the symmetric device. COMSOL models were created of the inlet reservoir with different sample inlet diameters showing that different inlet ratios developed distinct velocity profiles within the reservoir. These velocity profiles had direct effect on the initial separation of particles.

Experimentally it was determined that devices with outlet widths of 350 µm, a 2:1 inlet ratio, and placed at the top of the reservoir produced significant separation of three particle diameters. Downstream particle separation was related in plots with two separate dimensionless parameters, one using geometric ratios or Characteristic Sample Inlet (CSI). The other parameter developed using Comsol models of the distinct velocity profiles within the reservoir. Interestingly these plots using either dimensionless parameter had very similar trends. It is with an m_B/m_A value of 1.91 measured using COMSOL velocity profiles of the inlet reservoir that is critical for the initial separation of particles. Any combination of sample inlet diameter and inlet reservoir geometry, with appropriate flow rate able to generate an m_B/m_A value of 1.91, should theoretically separate different particle diameters along distinct streamlines in the reservoir. This should hold true regardless of the reservoir geometry or sample inlet position. In this project a 2:1 inlet ratio with a sample flow rate of 5 µl/hr was able to generate an m_B/m_A of 1.91 and thus effective separation. Lastly, the project goal of passively separating different sized particle diameters in a microfluidic chip was accomplished.

References

[1.] Gomez, F. A., 2008. Biological Applications of Microfluidics. *Wiley-Interscience*, pp.1 - 7.

[2.] Beebe, D. J., Mensing, G. A., Walker, G. M., 2002. Physics and Applications of Microfluidics in Biology. *Annual Reviews of Biomedical Engineering*. 4: pp. 261-286.

[3.] Duffy, D. C., McDonald, J. C., Schueller O. J. A., and Whitesides, G. M., 1998. Rapid Prototyping of Microfluidic Systems in Poly(dimethylsiloxane). *Analytical Chemistry*. 70: pp. 4974 - 4984.

[4.] Whitesides, G. M., 2006. The Origins and Future of Microfluidics. *Nature*. 442: 368 - 373.

[5.] McDonald, J. C., and Whitesides, G. M., 2002. Poly(dimethylsiloxane) as a Material for Fabricating Microfluidic Devices. *Accounts of Chemical Research*, 35(7): pp. 491 - 499.

[6.] Gomez-Sjoberg, R., Leyrat, A. A.,Pirone, D. M., Chen, C. S., Quake, S. R., 2007. Versatile, Fully Automated, Microfluidic Cell Culture System. *Analytical Chemistry*.79 (22), pp. 8557 - 8567.

[7.] Hansen, C. L., Skordalakes, E., Berger, J. M. & Quake, S. R., 2002. A robust and scalable microfluidics metering method that allows protein crystal growth by free interface diffusion. *PNAS,* 99, pp. 16531 - 16536.

[8.] Wainright, A., Nguyen, U. T., Bjornson, T. & Boone, T. D., 2003. Preconcentration and separation of double stranded DNA by electrophoresis in plastic microfluidic devices. *AnalyticalChemistry*. 24(21), pp. 3784 - 3792.

[9.] Park, Jae-Sung., and Jung, Hyo-II., 2009. Multiorifice Flow Fractionation: Continuous Size-Based Separation of Microspheres Using a Series of Contraction/Expansion Microchannels. *Analytical Chemistry*. 81(20), pp. 8280 - 8288.

[10.] Arora, A., Simone, G. Salieb-Beugelaar, G. B., Kim, J. T., and Manz, A., 2010. Latest Devolopments in Micro Total Analysis System. *Analytical Chemistry*. 82 (12), pp. 4830 - 4847.

[11.] Pamme, N., 2007. Continuous flow separation in microfluidic devices. *Lab on Chip*. 7, pp. 1644 - 1659.

[12.] Bahgat, A. A. S., Kuntaegowdanahalli, S. S., and Papautsky, I., 2008. Continuous particle separation in spiral microchannels using dean flows and differential migration. *Lab on a Chip*.8, pp. 1906 - 1914.

[13.] Yamada, M., Seki., M., 2006. Microfluidic Cell Sorter Employing Flow Splitting and Recombining. *Analytical Chemistry*.78, pp. 1357-1362.

[14.] Emmelkamp, J., Wolbers, F., Andersson, H., DaCosta, R. S., Wilson, B. C., Vermes, I., Berg van den, A., 2004.The potential of autofluorescence for the detection of single living cells for label-free cell sorting in microfluidic systems. *Electrophoresis*. 25 (21-22). pp. 3740 - 3745.

[15.] Wolff, A., Perch-Nielsen, I. R., Larsen, U. D., Friis, P., Goranovic, G., Poulsen, C. R., Kutter, J. P.,Telleman, P., 2003. Integrating advanced functionality in a microfabricated high-throughput fluorescent-activated cell sorter*. Lab on a Chip**. 3, pp. 22 - 27.

[16.] Takahashi, K., Hattori, A., Suzuki, I., Ichiki, T., Yasuda, K., 2004. Non-destructive on-chip cell sorting system with real-time microscopic image processing. Journal of Nanobiotechnology. 2: 9.

[17.] Gascoyne, P., Mahidol, C.,Ruchirawat, M., Satayavivad, J., Watcharasit, P., Becker, F. F., 2002.Microsample preparation by dielectrophoresis: isolation of malaria. *Lab on a Chip*. 2, pp. 70 - 75.

[18.] Wang, M. M., Tu, E., Raymond, D. E., Yang, J. M., Zhang, H. C., Hagen, N., Dees, B., Mercer, E. M., Forster, A. H., Kariv, I., Marchand, P. J., Butler,W. F., 2005. Microfluidic sorting of mammalian cells by optical force switching. *Nature Biotechnology,* 23, pp. 83 - 87.

[19.] Yamada, M., Nakashima, M., Seki, M., 2004. Pinched flow fractionation: continuous size separation of particles utilizing a laminar flow profile in a pinched microchannel. *Analytical Chemistry*, 76(18), pp. 5465 - 5471.

[20.] Bahgat, A. A. S., Sathyakumar, S., Kuntaegowdanahalli, S. S., and Papautsky, I., 2008. Enhanced particle filtration using shear-modulated inertial migration. *Physics of Fluids*, 20, pp. 101702.

[21.] Squires, T. M., Quake, S. R., 2005. Microfluidics: Fluid physics at the nanoliterscale. *Review of Modern Physics*,**7**, pp. 977 - 1026.

[22.] Henrik, B., 2008. Theoretical Microfluidics. *Oxford University Press, USA*, pp. 1 - 6.

[23.] Di Carlo, D., Irimia, D., Tompkins, R.G., and Toner, M., 2007. Continuous inertial focusing, ordering, and separation of particles in microchannels. *PNAS,* 105(48), pp. 18892 - 18897.

[24.] Takagi, J., Yamada, M., Yasuda, M., and Seki, M. 2005. Continuous particle separation in a microchannel having asymmetrically arranged multiple branches. *Lab on a Chip,* 5, pp. 778 - 784.

[25.] Weibel, D. B., Diluzio, W. R., Whitesides, G. M., 2007. Microfabrication meets microbiology. *Nature Reviews Microbiology*, 5(3): p. 209 - 218.

[26.] Lorenz, H., Despont, M., Fahrni, N., LaBianca, N., Renaud, P., and Vettiger, P., 1997. SU-8: A Low- Cost Negative Resist for MEMS. *Journal of Micromechanical Microengineering*, 7: 121 - 124

[27.] Campo, A., and Greiner, C., 2007. SU-8: A Photoresist for High-Aspect-Ratio and 3D Submicron Lithography. *Journal of Micromechanical Microengineering*, 17: R81 - R95.

[28.] Younan, X., Whitesides, G.M., 1998. Soft Lithography.*Annual Review of Materials Science*, 37: pp. 550 - 575.

[29.] Voldman, J., Gray, M. L., Schmidt, M. A., 1999. Microfrabrication in Biology and Medicine. *Annu Rev. Biomed. Eng*, 01: pp. 401 - 425.

[30.] Middleman, S., 1993. Process Engineering: Analysis in Semiconductor Device Fabrication. *Mcgraw-Hill College*, pp. 313 - 320.

[31.] MicroChem. Nano SU-8. Negative Tone Photoresist Formulation 50-100, Pages 1 - 2.

[32.] Mata, A., Fleischman, A. J., Roy, S., 2005. Characterization of Polydimethylsiloxane (PDMS) Properties for Biomedical Micro/Nanosystems. *Biomedical Devices*. 7(4): 281 - 293.

[33.] Sia, S.K., Whitesides, G.M., 2003. Microfluidic Devices Fabricated in Poly(dimethylsiloxane) for Biological Studies. *Electrophoresis*. 24: 3563 - 3576.

[34.] Lee, J. N., Park, C., and Whitesides, G. M., 2003. Solvent Compatibility of Poly(dimethylsiloxane)- Based Microfluidic Devices. *Analytical Chemistry*. 75: 6544 - 6554.

[35.] Invitrogen FluoSpheres Fluorescent Microspheres. *Manuals and Protocols*, Pages 1 - 6.

V Appendix A

A.1 Table 6 and Table 7 One-way ANOVA Statistics

Below are the results of a One-way ANOVA with each outlet set as an experimental

unit and particle diameter set as the treatment. These are the statistical results used in

both Tables 6 and 7 in Sections 3.4 and 3.5 respectively. In Table 6 and Table 7, only

devices with *both* collection outlet widths of 350 μm and a 2:1 inlet ratio did a specific

particle diameter significantly separate to unique outlet (i.e. 10 μm particles to Outlet 1,

5.5 μm to Outlet 2, and 3.0 μm to Outlet 3). Particle separations were determined using

pure counting from video recordings, as described in Sections 2.3.4.

#1.) One-way ANOVA: Collection Outlet 1 versus Particle Diameter

```
Source      DF        SS       MS        F       P
Particle     2   4938.78  2469.39   493.07   0.000
Error      138    691.14     5.01
Total      140   5629.91

S = 2.238    R-Sq = 87.72%    R-Sq(adj) = 87.55%

                              Individual 95% CIs For Mean Based on
                              Pooled StDev
Level     N     Mean    StDev  -------+---------+---------+---------+--
10 μm     46   14.587   1.147                                    (*-)
3.0 μm    48    2.286   2.460   (-*)
5.5 μm    47    1.658   2.749  (*-)
                              -------+---------+---------+---------+--
                                 4.0       8.0      12.0      16.0

Grouping Information Using Tukey Method
Particle   N    Mean   Grouping
10 μm     46  14.587   A
3.0 μm    48   2.286     B
5.5 μm    47   1.658     B
Means that do not share a letter are significantly different.
```
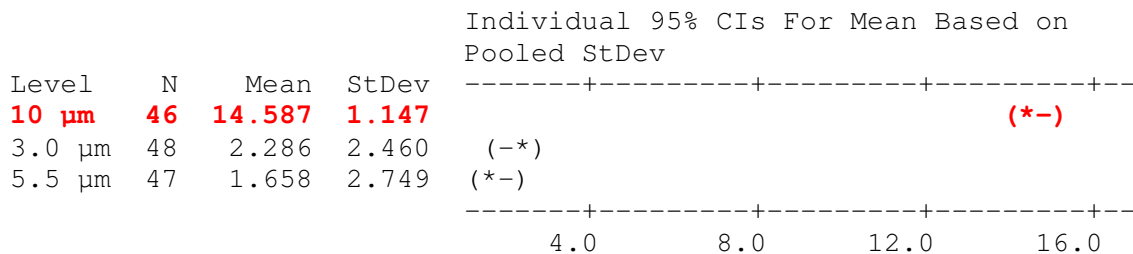
#2.) One-way ANOVA: Collection Outlet 2 versus Particle Diameter

```
Source      DF      SS      MS      F       P
Particle     2   1305.1   652.5   48.08   0.000
Error      138   1872.8    13.6
Total      140   3177.8


S = 3.684   R-Sq = 41.07%   R-Sq(adj) = 40.21%


                             Individual 95% CIs For Mean Based on
Pooled StDev
Level     N    Mean   StDev    +---------+---------+---------+--------
10 µm    46   3.558   4.012    (---*----)
3.0 µm   48   5.337   4.273         (---*----)
5.5 µm   47  10.734   2.512                                (---*---)
                              +---------+---------+---------+--------
                              2.5       5.0       7.5       10.0


Grouping Information Using Tukey Method
Particle   N     Mean  Grouping
5.5 µm    47   10.734  A
3.0 µm    48    5.337    B
10 µm     46    3.558    B
Means that do not share a letter are significantly different.
```
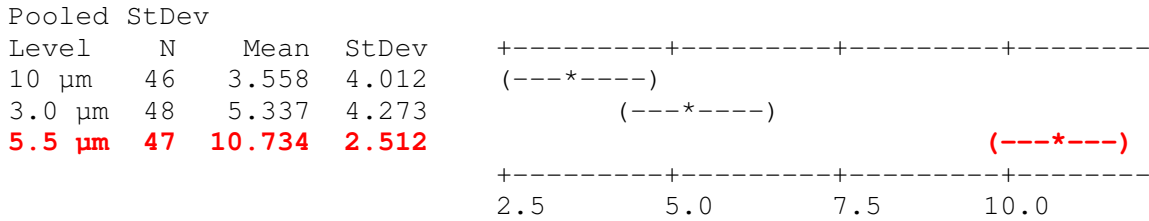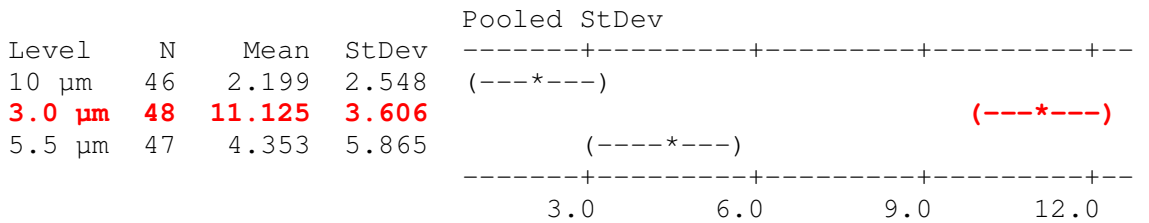
#3.) One-way ANOVA: Collection Outlet 3 versus Particle Diameter

```
Source      DF      SS       MS      F       P
Particle     2   2052.6   1026.3   56.98   0.000
Error      138   2485.6     18.0
Total      140   4538.2


S = 4.244   R-Sq = 45.23%   R-Sq(adj) = 44.44%


                             Individual 95% CIs For Mean Based on
                             Pooled StDev
Level     N    Mean   StDev  -------+---------+---------+---------+--
10 µm    46   2.199   2.548  (---*---)
3.0 µm   48  11.125   3.606                              (---*---)
5.5 µm   47   4.353   5.865        (----*---)
                             -------+---------+---------+---------+--
                                    3.0       6.0       9.0       12.0


Grouping Information Using Tukey Method
Particle   N     Mean  Grouping
3.0 µm    48   11.125  A
5.5 µm    47    4.353    B
10 µm     46    2.199      C
Means that do not share a letter are significantly different.
```

A.2 Table 7 Two-Sample T-test Statistics

Below are the results of a Two Sample T-test comparing particle distributions between the 2:1 inlet ratio and the 3.2:1 inlet ratio from Table 7 in Section 3.5. The three T-tests respectively compare 10 µm particles that distributed to Outlet 1 (see #1. below), 5.5 µm particles that distributed to Outlet 2 (see #2. below), and 3.0 µm particles that distributed to Outlet 3 (see #3. below). Only for 3.0 µm particles did distribution not significantly different between the 2:1 inlet ratio and the 3.2:1 inlet. For both 10 µm and 5.5 µm particles, distribution was significant between the two inlet ratios. Particle separations were determined using pure counting from video recordings, as described in Sections 2.3.4.

#1.) Two-Sample T-Test and CI: 2:1, Outlet 1, 10 um; 3.2:1, Outlet 1, 10 um

```
Two-sample T for 2:1, Outlet 1, 10 um vs 3.2:1, Outlet 1, 10 um

             N   Mean  StDev  SE Mean
2:1, Outlet 1, 10 um      46  14.59   1.15     0.17
3.2:1, Outlet 1, 10 um    44  11.86   2.02     0.30


Difference = mu (2:1, O1, 10 um) - mu (3.2:1, O1, 10 um)
Estimate for difference:  2.723
95% CI for difference:  (2.029, 3.418)
T-Test of difference = 0 (vs not =): T-Value = 7.82
```
P-Value = 0.000 DF = 67

#2.) Two-Sample T-Test and CI: 2:1, Outlet 2, 5.5 um, 3.2:1, Outlet 2, 5.5 um

```
Two-sample T for 2:1, Outlet 2, 5.5 um vs 3.2:1, Outlet 2, 5.5 um

                    N    Mean   StDev   SE Mean
2:1, Outlet 2, 5.5 um     47   10.73    2.51      0.37
3.2:1, Outlet 2, 5.5 um   50    8.40    3.17      0.45


Difference = mu (2:1, Outlet 2, 5.5 um) - mu (3.2:1, Outlet 2, 5.5
um)
Estimate for difference:  2.334
95% CI for difference:  (1.184, 3.484)
T-Test of difference = 0 (vs not =): T-Value = 4.03
```
P-Value = 0.000 ```DF = 92```

#3.) Two-Sample T-Test and CI: 2:1, Outlet 3, 3.0 um, 3.2:1, Outlet 3, 3.0 um

```
Two-sample T for 2:1, Outlet 3, 3.0 um vs 3.2:1, Outlet 3, 3.0 um

                    N    Mean   StDev   SE Mean
2:1, Outlet 3, 3.0 um     48   11.13    3.61      0.52
3.2:1, Outlet 3, 3.0 um   44    9.64    3.65      0.55


Difference = mu (2:1, O3, 3.0 um) - mu (3.2:1, O3, 3.0 um)
Estimate for difference:  1.489
95% CI for difference:  (-0.017, 2.995)
T-Test of difference = 0 (vs not =): T-Value = 1.96
```
P-Value = 0.053 ```DF = 89```

A.3. Table 9 Two-Sample T-test Statistics

Below are the results of a Two Sample t-test comparing particle distributions between the top and middle inlet position of a 2:1 inlet ratio. These are the statistical results used in in Table 9 and 7 in Sections 3.10. The three t-tests again respectively compare 10 µm particles that distributed to Outlet 1 (see #1. below), 5.5 µm particles that distributed to Outlet 2 (see #2. below), and 3.0 µm particles that distributed to Outlet 3 (see #3. below). Only for 3.0 µm particles did distribution not significantly different between the top and middle inlet position. For both 10 µm and 5.5 µm particles, distribution was significant between the two positions. Particle separations were determined using pure counting from video recordings, as described in Sections 2.3.4.

#1.) Two-Sample T-Test and CI: 2:1, Top Inlet Position, 10 um, 2:1, Middle Inlet Position, 10 um

```
Two-sample T for 2:1, Top Inlet, 10 um vs 2:1, Middle Inlet, 10 um

                              N    Mean   StDev   SE Mean
2:1, Top Inlet, 10 um        46   14.59   1.15      0.17
2:1, Middle Inlet, 10 um     47    9.02   3.22      0.47


Difference = mu (2:1, Top Inlet, 10 um) - mu (2:1, Middle Inlet, 10
um)
Estimate for difference:  5.566
95% CI for difference:  (4.566, 6.565)
T-Test of difference = 0 (vs not =): T-Value = 11.15
```
P-Value = 0.000 DF = 57

#2.) Two-Sample T-Test and CI: 2:1, Top Inlet Position, 5.5 um, 2:1, Middle Inlet Position, 5.5 um

```
Two-sample T for 2:1, Top Inlet, 5.5 um vs 2:1, Middle Inlet, 5.5 um

                              N   Mean  StDev  SE Mean
2:1, Top Inlet, 5.5 um       47  10.73   2.51     0.37
2:1, Middle Inlet, 5.5 um    48   8.92   2.90     0.42


Difference = mu (2:1, Top Inlet, 5.5 um) - mu (2:1, Middle Inlet,
5.5 um)
Estimate for difference:  1.817
95% CI for difference:  (0.712, 2.923)
T-Test of difference = 0 (vs not =): T-Value = 3.27
P-Value = 0.002  DF = 91
```

#3.) Two-Sample T-Test and CI: Top Inlet Position, 3.0 um, 2:1, Middle Inlet Position, 3.0 um

```
Two-sample T for 2:1, Top Inlet, 10 um vs 2:1, Middle Inlet, 3.0 um

                            N   Mean  StDev  SE Mean
2:1, Top Inlet, 3.0 um     47  11.13   3.61     0.52
2:1, Middle Inlet, 3.0 um  48  12.10   2.87     0.41


Difference = mu (2:1, Top Inlet, 3.0 um) - mu (2:1, Middle Inlet,
3.0 um)
Estimate for difference:  -0.975
95% CI for difference:  (-2.287, 0.337)
T-Test of difference = 0 (vs not =): T-Value = -1.48
P-Value = 0.143  DF = 89
```